Stability of neutrino parameters and self-complementarity relation with varying SUSY breaking scale

K. Sashikanta Singh* and Subhankar Roy†
Physics Department, Gauhati University, Guwahati 781014, India

N. Nimai Singh‡
Physics Department, Manipur University, Manipur 795003, India

(Received 1 October 2017; published 27 March 2018)

The scale at which supersymmetry (SUSY) breaks (m_s) is still unknown. The present article, following a top-down approach, endeavors to study the effect of varying m_s on the radiative stability of the observational parameters associated with the neutrino mixing. These parameters get additional contributions in the minimal supersymmetric model (MSSM). A variation in m_s will influence the bounds for which the Standard Model (SM) and MSSM work and hence, will account for the different radiative contributions received from both sectors, respectively, while running the renormalization group equations (RGE). The present work establishes the invariance of the self complementarity relation among the three mixing angles, $\theta_{13} + \theta_{12} \approx \theta_{23}$ against the radiative evolution. A similar result concerning the mass ratio, $m_2 : m_1$ is also found to be valid. In addition to varying m_s, the work incorporates a range of different seesaw (SS) scales and tries to see how the latter affects the parameters.

DOI: 10.1103/PhysRevD.97.055038

I. INTRODUCTION

The physics of neutrino is going through a revolutionary period. From various recent experiments, a small but nonzero value of the reactor angle, θ_{13} is confirmed [1,2]. In addition to this, the Dirac CP phase, δ is also observed [3,4]. Recent experiments on neutrino oscillation, $0\nu\beta\beta$, and the cosmological observations have revealed precise and important results on the observational parameters like the three mixing angles (θ_{13}, θ_{12}, θ_{23}), two mass-squared differences (Δm^2_{21}, Δm^2_{31}) and possible upper bound on the sum of neutrino masses (Σm_i) etc. [5–7]. But still we are unable to understand the absolute value of neutrino masses, nature of neutrino mass hierarchy, or its type: Dirac/Majorana etc. The realization that neutrinos are massive in contrast to its old popular assumption that it is massless (according to the SM) is one of the strong signatures that the SM of particle physics has to be extended beyond its present horizon.

Most of the current studies on physics beyond the SM (BSM) relies on the possible existence of supersymmetry (SUSY). But there are other models of BSM physics which does not incorporate the idea of SUSY [8,9]. It is hypothesized that SUSY existed at the early stage of big bang. But with the expansion of our Universe SUSY gets broken and reduced to our present day SM. At what scale that breaking occurs is still an unknown but an important parameter. The general idea is that there are two possible energy scales for the SUSY breaking (m_s): low and high. The low m_s scale [10,11] is expected to be about a few TeV or so as suggested by the grand unified theory (GUT), whereas the high SUSY breaking scale is expected to be somewhere around 10^{12} GeV [12].

One significant finding from the recent LHC experiment which sounds a little disappointing towards the possibility of SUSY is that the experiment, which was operated at an energy scale of 13 TeV, has not provided any evidence of the existence of SUSY particles so far [13,14]. In SUSY inspired neutrino physics, it is predicted that SUSY plays an important role over the neutrino masses and other observational parameters [15–17]. The gauge coupling and Yukawa coupling constants suffer different radiative contributions from the MSSM and SM sectors. Similar to this, we expect that the neutrino observational parameters are also subjected to such kind of effects.

One of the reasons why the variation in m_s is expected to bring changes to various observational parameters is owing to the changes in the effective range of both MSSM and SM. When we increase the m_s scale, the effective range of SM increases, whereas that for MSSM decreases and vice versa. It will change the amount of radiative correction that each parameter receives from the SM and MSSM, respectively. In our previous work [18], we show the variation of

*Corresponding author.
ksm1skynet@gmail.com
†meetsubhankar@gmail.com
‡nimai03@yahoo.com

the unification point of the gauge couplings with varying m_s scale. Such behavior is likely to be seen for the neutrino oscillation parameters too. In this regard, it is important to study the possible effects of varying m_s on the radiative evolution of the neutrinos and hence, to determine (or narrow down) the possible range of m_s scale.

The possible reason behind the suppression of SUSY motivated effects at the LHC experiments may be due to the low luminosity of the beam. By the end of 2012, LHC's integrated luminosity, running at a center-of-mass energy $\sqrt{s} = 8$ TeV, is already over 20 fb^{-1} [19]. The present integrated luminosity of the LHC for $\sqrt{s} = 13$ TeV is 35.9 fb^{-1} for CMS [20] and 36.1 fb^{-1} for ATLAS [21]. Some predicted the required integrated luminosity for observing SUSY related events to be 3000 fb^{-1} [22,23], which is approximately 85 times greater than the present luminosity. Nevertheless, this still gives us a hope for the possible existence of $m_s < 13$ TeV. If a seesaw (SS) mechanism is the only cause behind the generation of small neutrino masses, then it appears that the right-handed neutrino mass scale must lie somewhere within the range of $(10^{10} - 10^{16})$ GeV [24,25]. In our analysis, we shall vary the SS scale starting from 10^{10}–10^{15} GeV.

One sees that the numerical range of three mixing angles within 1σ [1] appears as in the following:

$$\theta_{13} = 8.44^{0+0.16}_{-0.17}, \quad \theta_{12} = 34.5^{0+1.1}_{1.0}, \quad \text{and} \quad \theta_{23} = 41.0^{0+1.1}_{-1.1}. \tag{1}$$

We see that there may lie a self-complementarity (SC) among these parameters in terms of the following relation:

$$\theta_{23} = q \times (\theta_{13} + \theta_{12}), \tag{2}$$

where the parameter, q, is either unity or $\mathcal{O}(1)$. The self-complementarity relation (SC) is an important phenomenological relation [26,27] similar to the quark-lepton complementarity relations [28–30]. The possible existence of such relations among the parameters are expected to be the signatures of a certain flavor symmetry working in the background. The present analysis attempts not to deal with the possible origin of such a kind of a SC relation, rather it insists on the existence of such a relation even at higher energy scale. Our work starts with an assumption that this SC relation holds good at the SS scale. Through our analysis, we will show that this relation remains invariant against the radiative evolution for varying the m_s and SS scale. We emphasize that similar to the works in the literature which focus only on the renormalization group invariant parameters [31–35], the SC relation can also serve as an RGE invariant relation.

The present investigation is a continuation of our previous work [18], where we studied the radiative evolution of the three gauge, third generation Yukawa, and quartic Higgs couplings following a bottom-up approach, with varying the SUSY breaking scale m_s. It was observed that the unification scales for both the gauge couplings and Yukawa couplings vary but in the opposite trend and tend to attain a fixed value with increasing m_s. There, we vary m_s starting from 500 GeV to 7 TeV. However, in the present work, we follow the top down approach starting from the seesaw scale up to the electroweak scale. We fix, $\tan\beta = 58.6$, which is relevant in the context of our previous work [18].

This paper is organized in the following order. In Sec. II, we give a brief discussion of the neutrinos RGEs. In Sec. III, we study the possible radiative effects on the neutrino parameters at the weak scale. In Sec. IV, we present the numerical analysis. In Sec. V, we summarize our work, and in the Appendix, we give the RGEs for the gauge, Yukawa and quartic Higgs couplings in two loops for both the SM and MSSM.

II. RGES FOR NEUTRINO PARAMETERS

Renormalization group approach is a tool for studying physics at a different energy scale, which are otherwise impossible to reach with the current technology, and then to compare it with the available low energy data. Radiative analysis of neutrino parameters requires the RGEs of gauge couplings, Yukawa couplings, and the quartic Higgs couplings. The radiative properties of these couplings have been studied extensively in different models, and these three gauge couplings are expected to be unified at an energy scale approximately at 2×10^{16} GeV [36–41]. The RGEs for the gauge couplings, Yukawa couplings, and quartic Higgs coupling are given in the Appendix. We use 2-loops RGEs for both the SM and MSSM.

The RGE analysis of the neutrino parameters can be done in two possible ways viz.: i) by a run and diagonalize method: where the whole neutrino mass matrix is allowed to evolve using their appropriate RGEs, and then the corresponding neutrino parameters can be achieved at the desirable energy scale (μ) by diagonalizing the neutrino mass matrix, ii) by using the RGEs of the corresponding neutrino parameters separately as defined by the Eqs. (3) to (13). In both the cases, the RGEs of all the neutrino parameters and the RGEs of various coupling parameters are required to be solved simultaneously. In this work, we adopt the later stand.

The input parameters for the gauge, Yukawa, and, quartic Higgs couplings at the seesaw scale, given in Table I, are taken form our previous work [18]. In the present analysis, we choose our starting energy scale to be the SS scale. We consider a different possible SS scale starting from 10^{10} GeV to 10^{15} GeV, and we run down all the observational neutrino parameters from SS scale up to the electroweak scale ($m_Z = 91.18$ GeV) via m_s, which also varies in our analysis.

TABLE I. Input values for gauge, Yukawa, and quartic Higgs couplings [18].

Gauge couplings	Yukawa couplings	Quartic-Higgs couplings
g_1—0.6032	y_t—0.76809	λ—0.58
g_2—0.6826	y_b—0.80488	⋯
g_3—0.7557	y_τ—0.91448	⋯

The radiative properties of neutrinos has been studied extensively in various models [41–50]. The standard two loops RGEs for the neutrino masses, mixings, and *CP* phases are shown below. For the three neutrino mixing angles [41], the RGEs are

$$\dot{\theta}_{12} = -\frac{Cy_\tau^2}{32\pi^2}\sin 2\theta_{12}s_{23}^2\frac{|m_1 e^{i\psi_1} + m_2 e^{i\psi_2}|^2}{\Delta m_{21}^2}, \tag{3}$$

$$\begin{aligned}\dot{\theta}_{13} = &-\frac{Cy_\tau^2}{32\pi^2}\sin 2\sin 2\theta_{23}\frac{m_3}{\Delta m_{31}^2(1+\xi)}\\ &\times[m_1\cos(\psi_1-\delta) - (1+\xi)m_2\cos(\psi_2-\delta)\\ &-\xi m_3\cos\delta],\end{aligned} \tag{4}$$

$$\begin{aligned}\dot{\theta}_{23} = &-\frac{Cy_\tau^2}{32\pi^2}\sin 2\theta_{23}\frac{1}{\Delta m_{31}^2}\\ &\times\left[c_{12}^2|m_2 e^{i\psi_2} + m_3|^2 + s_{12}^2\frac{|m_1 e^{1\psi_2} + m_3|^2}{(1+\xi)}\right],\end{aligned} \tag{5}$$

where, $\Delta m_{21}^2 = m_2^2 - m_1^2$ and $\Delta m_{31}^2 = m_3^2 - m_1^2$, $\xi = \frac{\Delta m_{21}^2}{\Delta m_{31}^2}$.

The RGEs for the three phases are (for Dirac phase)

$$\dot{\delta} = \frac{Cy_\tau^2}{32\pi^2}\frac{\delta^{(-1)}}{\theta_{13}} + \frac{Cy_\tau^2}{8\pi^2}\delta^0, \tag{6}$$

where

$$\begin{aligned}\delta^{(-1)} = &\sin 2\theta_{12}\sin 2\theta_{23}\frac{m_3}{\Delta m_{31}^2(1+\xi)}\\ &\times[m_1\sin(\psi_1\delta) - (1+\xi)m_2\sin(\psi_2-\delta) + \xi m_3\sin\delta],\end{aligned} \tag{7}$$

$$\begin{aligned}\delta^{(0)} = &\frac{m_1 m_2 s_{23}^2\sin(\psi_1-\psi_2)}{\delta m_{21}^2}\\ &+ m_3 s_{12}^2\left[\frac{m_1\cos 2\theta_{23}\sin\psi_1}{\Delta m_{31}^2(1+\xi)} + \frac{m_2 c_{23}^2\sin(2\delta-\psi_2)}{\Delta m_{31}^2}\right]\\ &+ m_3 c_{12}^2\left[\frac{m_1 c_{23}^2\sin(2\delta-\psi_1)}{\Delta m_{31}^2(1+\xi)} + \frac{m_2\cos 2\theta_{23}^2\sin(\psi_2)}{\Delta m_{31}^2}\right],\end{aligned} \tag{8}$$

(for Majorana phases)

$$\begin{aligned}\dot{\psi}_1 = &\frac{Cy_\tau^2}{8\pi^2}\left\{m_3\cos 2\theta_{23}\frac{m_1 s_{12}^2\sin\psi_1 + (1+\xi)m_2 c_{12}^2\sin\psi_2}{\Delta m_{31}^2(1+\xi)}\right.\\ &\left.+\frac{m_1 m_2 c_{12}^2 s_{23}^2\sin(\psi_1-\psi_2)}{\Delta_{21}^2}\right\},\end{aligned} \tag{9}$$

$$\begin{aligned}\dot{\psi}_2 = &\frac{Cy_\tau^2}{8\pi^2}\left\{m_3\cos 2\theta_{23}\frac{m_1 s_{12}^2\sin\psi_1 + (1+\xi)m_2 c_{12}^2\sin\psi_2}{\Delta m_{31}^2(1+\xi)}\right.\\ &\left.+\frac{m_1 m_2 s_{12}^2 s_{23}^2\sin(\psi_1-\psi_2)}{\Delta_{21}^2}\right\}.\end{aligned} \tag{10}$$

The RGEs for the neutrino mass eigenvalues are

$$\dot{m_1} = \frac{1}{16\pi^2}[\alpha + Cy_\tau^2(2s_{12}^2 s_{23}^2 + F_1)]m_1, \tag{11}$$

$$\dot{m_2} = \frac{1}{16\pi^2}[\alpha + Cy_\tau^2(2c_{12}^2 s_{23}^2 + F_2)]m_2, \tag{12}$$

$$\dot{m_3} = \frac{1}{16\pi^2}[\alpha + 2Cy_\tau^2 c_{13}^2 c_{23}]m_3, \tag{13}$$

where

$$F_1 = -s_{13}\sin 2\theta_{12}\sin 2\theta_{23}\cos\delta + 2s_{13}^2 c_{12}^2 c_{23}^2, \tag{14}$$

$$F_2 = s_{13}\sin 2\theta_{12}\sin 2\theta_{23}\cos\delta + 2s_{13}^2 s_{12}^2 s_{23}^2, \tag{15}$$

$$\left.\begin{aligned}\alpha &= -\tfrac{6}{5}g_1^2 - 6g_2^2 + 6y_t^2\\ C &= 1\end{aligned}\right\}\text{for MSSM} \tag{16}$$

$$\left.\begin{aligned}\alpha &= -3g_2^2 + 2y_\tau^2 + 6y_t^2 + 6y_b^2\\ C &= \tfrac{1}{2}\end{aligned}\right\}\text{for SM.} \tag{17}$$

With all the necessary mathematical frameworks in hand, we can now study the radiative nature of neutrino masses, mixings, and *CP* phases using the top-down running approach together with the MSSM unification conditions.

In the first step, all the parameters are allowed to run down from the seesaw scale to the SUSY breaking scale using their respective MSSM RGEs and from the SUSY breaking scale further down to the electroweak scale using their SM RGEs. At the transition point from MSSM to SM, we apply appropriate matching conditions as shown below,

$$g_i(M_{\rm SUSY}^-) = g_i(M_{\rm SUSY}^+), \tag{18}$$

$$\lambda_t(M_{\rm SUSY}^-) = \lambda_t(M_{\rm SUSY}^+)\sin\beta, \tag{19}$$

$$\lambda_b(M_{\rm SUSY}^-) = \lambda_b(M_{\rm SUSY}^+)\cos\beta, \tag{20}$$

$$\lambda_\tau(M_{\rm SUSY}^-) = \lambda_\tau(M_{\rm SUSY}^+)\cos\beta, \tag{21}$$

where $\tan\beta = v_u/v_d$ such that $v_u = v\sin\beta$, $v_d = v\cos\beta$, and $v = 246$ GeV is the vacuum expectation value of the

Higgs field. In our analysis, we choose a single SUSY spectrum for simplicity and study the radiative stability of the neutrino parameters at the weak scale for varying m_s.

III. RADIATIVE EFFECTS ON THE NEUTRINO OSCILLATION PARAMETERS AND THE *CP* PHASES

The radiative effects on the neutrino parameters for a strict normal or inverted hierarchy is small. If the neutrinos masses have a quasidegenerate spectrum, then the RG evolution between the lowest seesaw scale and electroweak energy scale can have sizable effects [51–54] on the neutrino oscillation parameters. The RG effects may even account for the difference between the mixings in the quark and the lepton sectors [55].

In MSSM, both the atmospheric (θ_{23}) and solar mixing angle (θ_{12}) increase with the decrease in energy as predicted by Eq. (3) and Eq. (4). Out of the three mixing angles, the solar mixing angle is prone to the largest RG effects because of the presence of a small Δm^2_{31} in the denominator, whereas θ_{13} is subjected to the smallest RG effect.

In the top-down approach, all the three mass eigenvalues behave in a similar fashion, and they all decrease with the decrease in energy scale. Because of the comparatively larger value of α with respect to y_t, y_b, and y_τ, the RG running effect on the mass eigenvalues is less. But, due to the same factor α, there is appreciable running in the RGEs of the mass eigenvalues in the SM case. The running of the mass eigenvalues in the MSSM is defined by a common scaling factor, except for the case of a large $\tan\beta$ where it deviates considerably.

For nearly degenerate neutrino masses and a large $\tan\beta$, the radiative influence of *CP* phases over other parameters becomes important. All of the phases (both Majorana and Dirac) undergo radiative correction. For different sets of the input phases, the RG effects on the neutrino oscillation parameters may differ. In the context, when the two Majorana phases are equal [41], the evolutions of the parameters are highly suppressed since the leading terms in the RGEs of the phases become zero [See Eq. (10) and Eq. (11)].

IV. NUMERICAL ANALYSIS AND THE RESULTS

The RGEs are differential equations and demand the input values for the parameters to be sought out, at the very outset. In our case, the starting point is the SS scale, and finally, we end up at the EW scale. From the SS scale up to the m_s scale, the RGEs follow a certain pattern [Eq. (16)] and revert to another form in the region from m_s up to the EW scale [Eq. (17)]. Both the SS scale and m_s are unknown to us. Our present analysis although tries to visualize the effect on the neutrino observational parameters for varying m_s, yet gives emphasis on the choice of the SS scale also. We fix the m_s values in between 1 TeV to 13 TeV. In addition, the SS scale is also assigned certain fixed values between 10^{10} GeV to 10^{15} GeV.

The parameters, g_1, g_2, g_3, y_t, y_b, y_τ, and λ are specified as per Table I. In the present analysis, we have got nine free parameters: m_1, m_2, m_3, θ_{13}, θ_{23}, θ_{12}, δ, ψ_1, and ψ_2. As stated earlier, the present study presumes the existence of the SC relation [see Eq. (2)] at the SS scale. By virtue of this relation, we assign initial input values only to θ_{13} and θ_{12}. Further simplifications are made regarding the initial choice of ψ_1 and ψ_2, which are constrained to be equal, $(\psi_1)_0 = (\psi_2)_0$, for all subsequent calculations [the notations $(\ldots)_0$ represent the initial input value of the parameter within the bracket]. In that way, we assign input values only to six neutrino observational parameters. To simplify, we summarize our strategy in the following way,

(Step 1) We vary the initial values of the six neutrino parameters at a fixed m_s scale. To ensure that the initial choice of the parameters beget the numerical values at the EW scale which are consistent within a 3σ range, we follow a simple mechanism. To illustrate, let us fix m_s at 5 TeV, the SS scale at 10^{14} GeV, and assume $(m_2)_0 = 2.34 \times 10^{-2}$ eV and $(\delta)_0 = 90°$. The remaining parameters, $(\theta_{13})_0$, $(\theta_{23})_0$, $(m_1)_0$, $(m_3)_0$, and $(\psi_1)_0$ are assigned with certain numerical values, so that the final output at the EW scale lies within 3σ. Next, we vary the parameter, $(\psi_1)_0$ and see how the remaining parameters, like, $(\theta_{ij})_0$ and $(m_i)_0$, are to be adjusted in order to keep the outcome within the 3σ range. For details, see Table II, Figs. 1(a) and 1(b). We see that, except $(m_3)_0$ which varies a little, the other input parameters are almost stable against changing $(\psi_1)_0$. The motivation behind performing this step is to ensure that the final numerical values in concern with the neutrino observational parameters are not too sensitive to the initial input of the Majorana phase. This observation helps us to choose an arbitrary value for $(\psi_1)_0$. We take $(\psi_1)_0 = 45°$ for all subsequent calculations.

(Step 2) The SUSY breaking scale m_s, is attributed to the following numerical values like, $1, 3, 5, \ldots 13$ TeV, and in accordance with that, we categorize seven sets of input values as, $A1, A3, A5 \ldots A13$, respectively. For example, the set A_5 corresponds to the set of input $(\theta_{ij})_0$, $(m_i)_0$, $(\delta)_0$, and $(\psi_1)_0$, at $m_s = 5$ TeV. For all the above mentioned sets, we fix $(\delta)_0 = 90°$. Similarly, we assign sets, $B1, B3, B5 \ldots B13$ with $(\delta)_0 = 270°$. This is to be noted that both kinds of sets Aj and Bj are the input values of the neutrino parameters, at the SS scale of 10^{14} GeV. There is another $\mathcal{O}(1)$ parameter, q which appears in Eq. (2) is tuned between 0.95 to 0.97. For details, see Table III.

(Step 3) In this step, keeping a certain input set, say $A5$ fixed, we vary the m_s scale between 1 TeV to 13 TeV, and check the stability of the neutrino observational parameters at the EW scale. The details are shown in the Tables IV–XI.

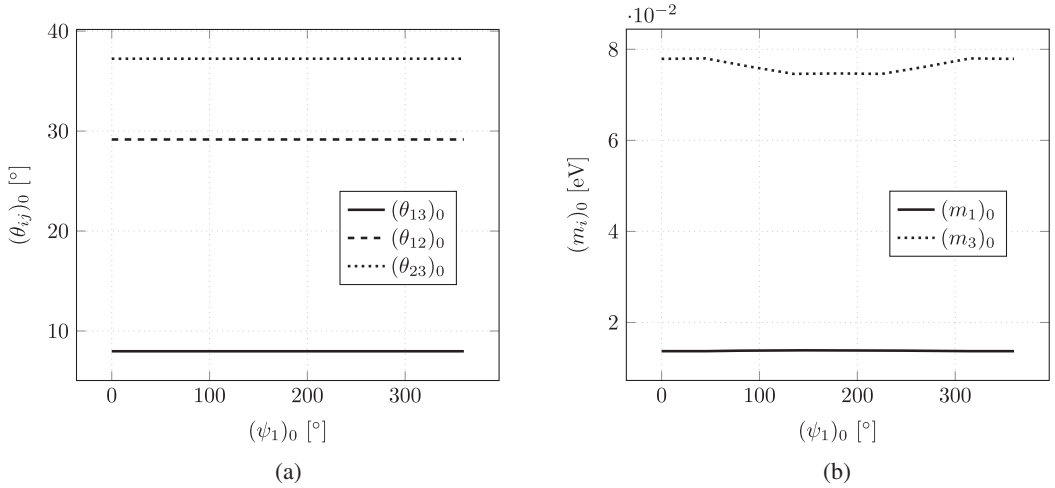

FIG. 1. (a) The variation of the $(\theta_{ij})_0$ against $(\psi_i)_0$ is shown. (b) The stability of $(m_i)_0$ against $(\psi_i)_0$ is studied. In our calculations, we assume the Majorana parameters to be equal. The m_s and SS scale are fixed at 5 TeV and 10^{14} GeV, respectively. The other initial input, $(\delta)_0 = 90°$ and $(m_2)_0 = 2.34 \times 10^{-2}$ GeV. The purpose of this study is to achieve the numerical values of the parameters at the EW scale within 1σ.

(Step 4) We repeat step 3, for different values of the SS scale, such as $10^{10}, 10^{11} \ldots 10^{15}$ GeV.

We will now discuss the results of our analysis.

A. For varying m_s at fixed SS scale

We keep track of the numerical values of the neutrino observational parameters at the EW scale. From Tables IV–XI, one sees that, except Δm^2_{21}, other parameters like θ_{13}, θ_{12}, θ_{23}, and Δm^2_{31} show stability at the face of the changing m_s. For all the three mixing angles, the fluctuations are consistent within 3σ bound [1]. But for Δm^2_{31}, the fluctuations sometimes cross the 3σ bound. Although the input entries corresponding to different neutrino parameters are almost the same for all the sets Aj and Bj, the solar mass squared difference at the EW scale is found quite sensitive towards both the initial input as well as to the m_s scale. To illustrate, one can see that for the input data set, say $A5$, results in $\Delta m^2_{21} = 7.57 \times 10^{-5}$ eV^2, and this is consistent within 1σ bound, for m_s being set at 5 TeV. If m_s is changed a little, say to 3 TeV and 7 TeV, we see that for the same input data set $A5$, the Δm^2_{21} become 9.16×10^{-5} and 6.67×10^{-5} eV^2, respectively. This output lies strictly outside the 3σ region. However, if we achieve an acceptable Δm^2_{21}, against a higher m_s scale, we can expect a little stability. To exemplify, if for $A11$, we achieve $\Delta m^2_{21} = 7.54 \times 10^{-5}$ eV^2 (within 1σ bound), against $m_s = 11$ TeV, then changing the m_s to either 9 or 13 TeV will not take this parameter outside 3σ. In addition, both solar and atmospheric mass squared difference decreases, with the increase in m_s scale. The charge conjugation and parity (CP) violating phases also vary a little if m_s were changed. With the increase of the latter, δ decreases, whereas the two Majorana phases increase [see Fig. 2].

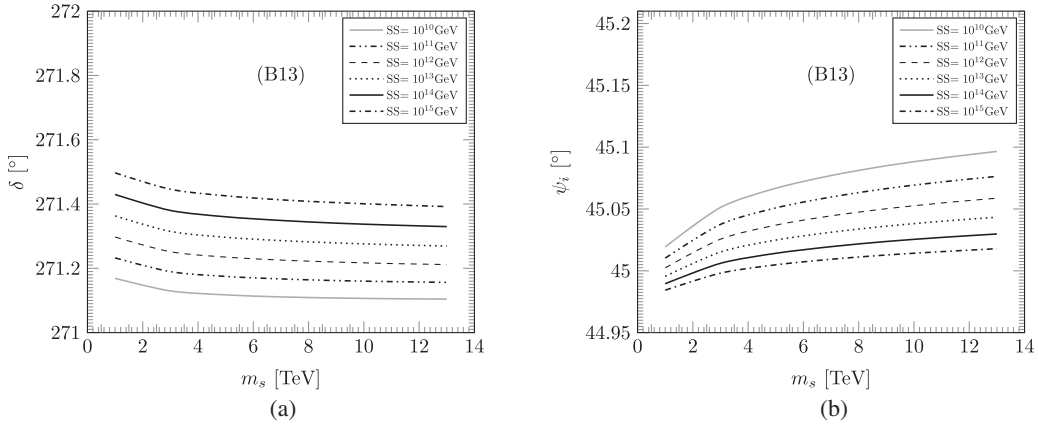

FIG. 2. The fluctuations of (a) the Dirac phase (δ) and (b) the Majorana phase (ψ_i) after RG evolution, at the EW scale, against changing m_s, and the SS scale are studied. m_s values are fixed at 1 Tev, 3 TeV, 5 Tev, 7 TeV, 9 Tev, 11 Tev, 13 TeV, and different SS scales are assumed at 10^{10} GeV, 10^{11} GeV, 10^{12} GeV, 10^{13} GeV, 10^{14} GeV, and 10^{15} GeV. Here, we consider only one input data set B13 as in Table III.

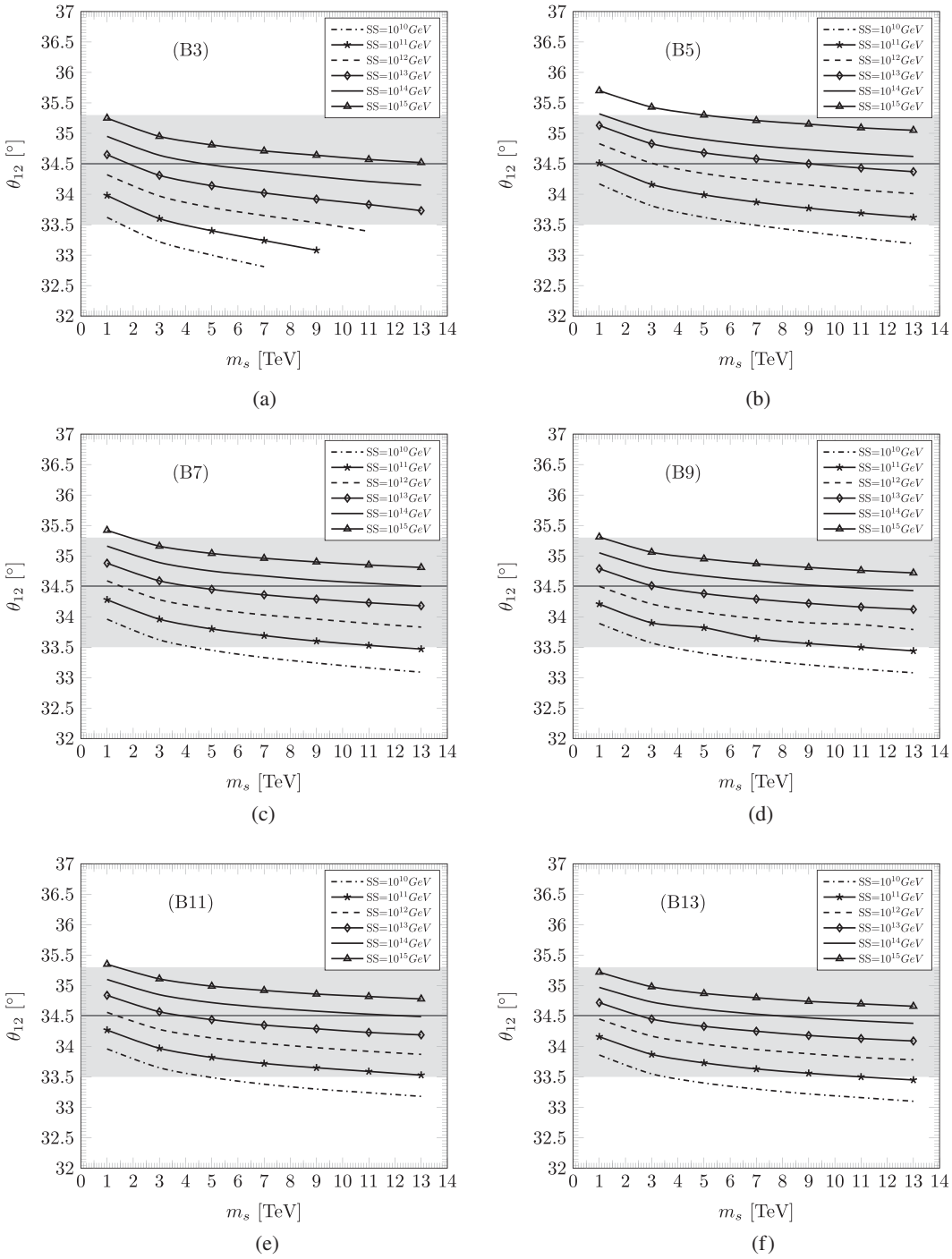

FIG. 3. The fluctuations of the numerical values of θ_{12}, at the EW scale is studied, against changing m_s, and SS scale. The shaded region (horizontal) represents the experimental 3σ range [1] and the horizontal bold line inside the shaded region indicates the best-fit value. The six figures (a), (b), (c), (d), (e), and (f) are for the different input data sets B3, B5, B7, B9, B11, and B13 respectively (as given in Table III). The SS scales are fixed at 10^{10} GeV, 10^{11} GeV, 10^{12} GeV, 10^{13} GeV, 10^{14} GeV, and 10^{15} GeV.

B. For varying m_s and SS scale

The discussion concerned so far is true only for the SS scale: 10^{14} GeV. We try to see how a changing SS scale, along with m_s, can affect the physical parameters at the EW scale as per the step (4) mentioned above. We note down the following. To exemplify, let us choose the input data set $B5$, which is capable of producing observable parameters at the EW scale consistent within 3σ, with m_s being fixed at 5 TeV, and the SS scale at 10^{14} GeV. With the SS scale fixed, first we vary m_s, and we get a certain plot, which

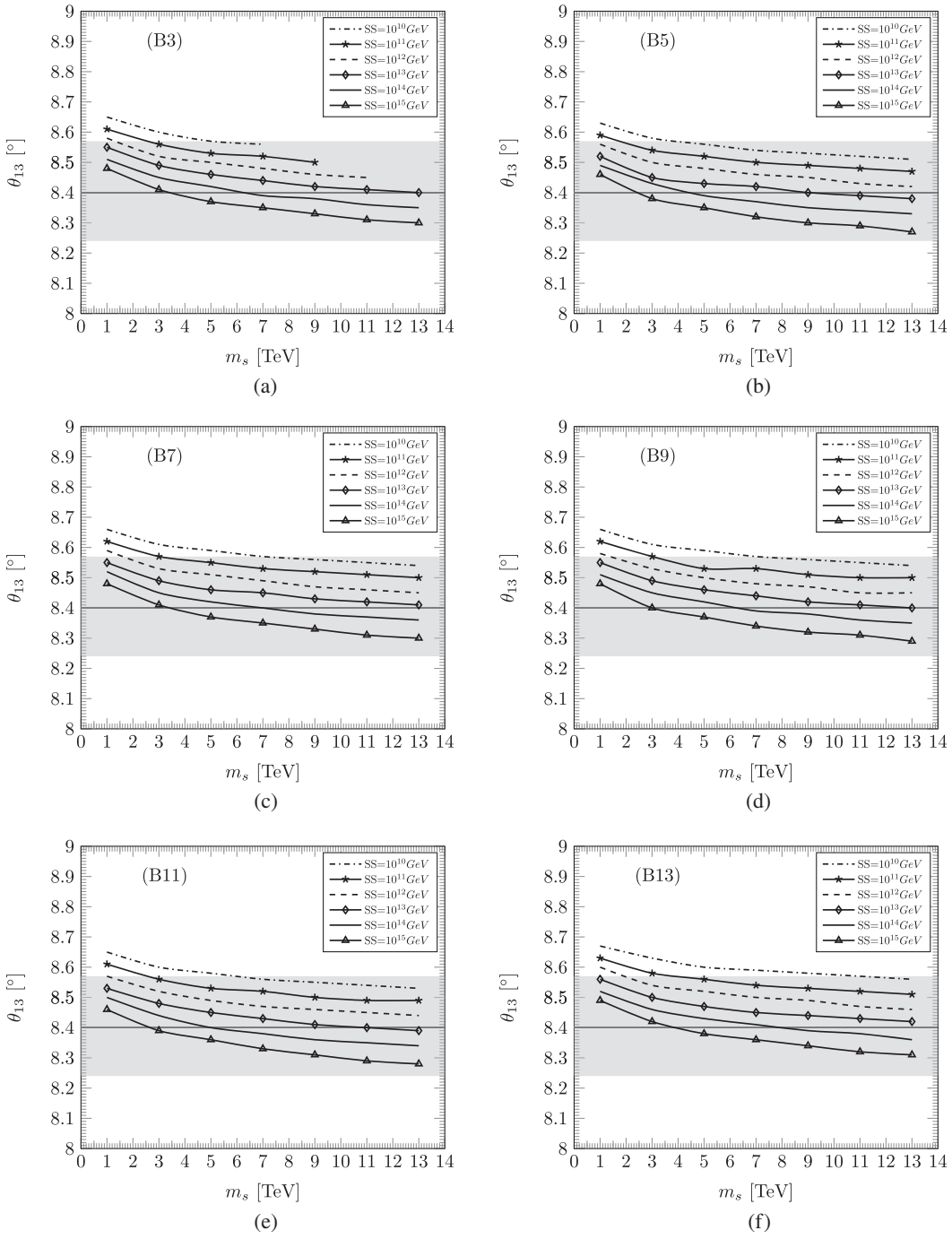

FIG. 4. The fluctuations of the numerical values of θ_{13}, at the EW scale is studied, against changing m_s, and the SS scale. The shaded region (horizontal) represents the experimental 3σ range [1], and the horizontal bold line inside the shaded region indicates the best-fit value. The six figures (a), (b), (c), (d), (e), and (f) are for the different input data sets B3, B5, B7, B9, B11, and B13 respectively (as given in Table III). The SS scales are fixed at 10^{10} GeV, 10^{11} GeV, 10^{12} GeV, 10^{13} GeV, 10^{14} GeV, 10^{15} GeV.

shows how the numerical value of that observable parameter at the EW scale changes against m_s. We redo the same to get another plot, but at a different SS scale, for same input data set. We observe the ascent or descent of the plots against the different SS scale.

(a) Among the three mixing angles, θ_{13}, the EW scale decreases if the SS scale is increased, whereas θ_{12} and θ_{23} increase. For wide ranges of the m_s and SS scale, the output values stay within the 3σ bound. However, for different input data sets concerned, the exclusion of certain m_s values or SS scales are also possible, depending upon the 3σ bound of the concerned mixing angles. For example, consider the case of θ_{12} at the EW scale, against a fixed input data set $B5$. If we

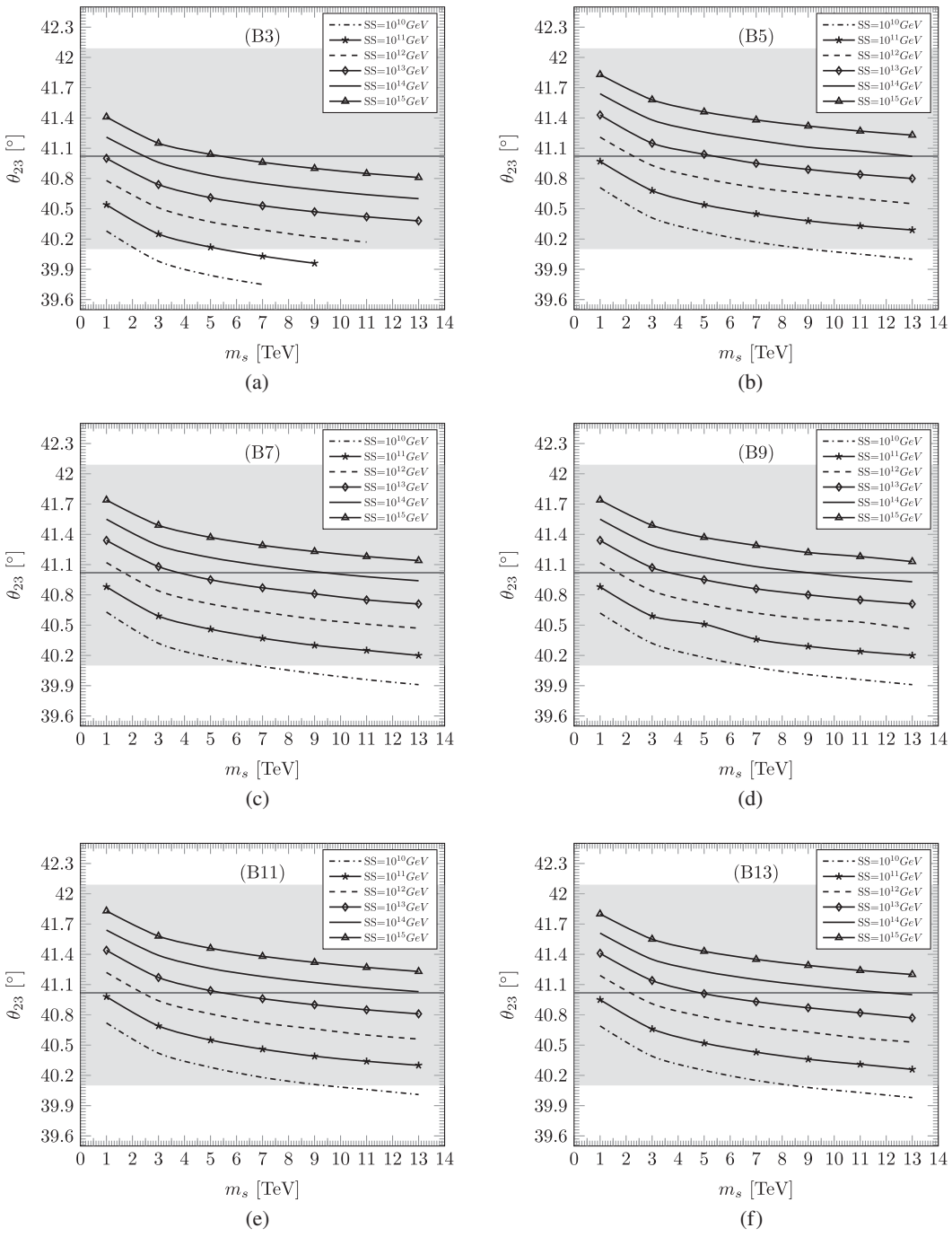

FIG. 5. The fluctuations of the numerical values of θ_{23}, at the EW scale is studied, against changing m_s, and the SS scale. The shaded region (horizontal) represents the experimental 3σ range [1], and the horizontal bold line inside the shaded region indicates the best-fit value. The six figures (a), (b), (c), (d), (e), and (f) are for the different input data sets B3, B5, B7, B9, B11, and B13 respectively (as given in Table III). The SS scales are fixed at 10^{10} GeV, 10^{11} GeV, 10^{12} GeV, 10^{13} GeV, 10^{14} GeV, and 10^{15} GeV.

believe the SS scale to be 10^{10} GeV, then, from the plots, it is evident that the SUSY breaking scale should not be more than 7 TeV [see Figs. 3]. For the other two mixing angles, (θ_{13}) and (θ_{13}), see Figs. 4 and 5, respectively.

(b) With all the conditions being the same as before, the δ increases if the SS scale is increased, whereas the reverse is true for the Majorana phases. [See Figs. 2a–2b].

(c) We observe certain interesting results in concern with Δm^2_{21} and Δm^2_{31}. The mass squared differences are found highly sensitive to the initial data set, m_s, and the SS scale. The Δm^2_{31} remains more or less stable against m_s, but crosses 3σ bound if the SS scale is

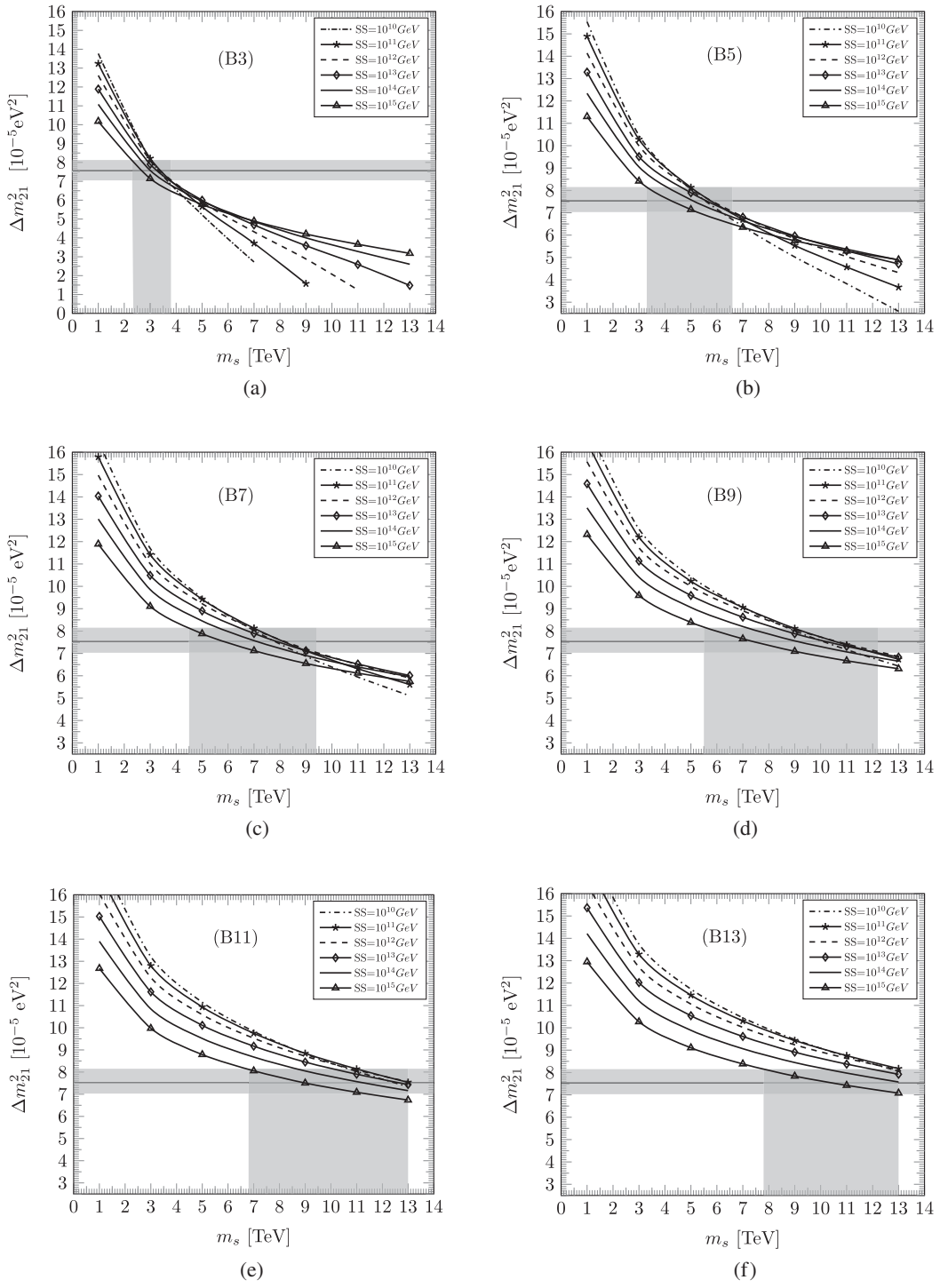

FIG. 6. The fluctuations of the numerical values of Δm^2_{21}, at the EW scale is studied, against changing m_s, and the SS scale. The shaded region (horizontal) represents the experimental 3σ range [1], and the horizontal bold line inside the shaded region indicates the best-fit value. The vertical shaded region corresponds to the allowed m_s region, for which the plots for different SS scale lie within the 3σ bound. The six figures (a), (b), (c), (d), (e), and (f) are for the different input data sets B3, B5, B7, B9, B11, and B13 respectively (as given in Table III). The SS scales are fixed at 10^{10} GeV, 10^{11} GeV, 10^{12} GeV, 10^{13} GeV, 10^{14} GeV, and 10^{15} GeV.

varied. On the contrary, the Δm^2_{21} fluctuates more with m_s but less with SS scale. It is interesting to note that against a fixed input data set (say, B5), with respect to 3σ range of Δm^2_{21}, one can even find a bound over the m_s scale. This bound shifts to the right, i.e., towards a higher m_s region as we take the input numerals as per the initial data sets from $B1$ to $B13$ (see Figs. 6 and 7).

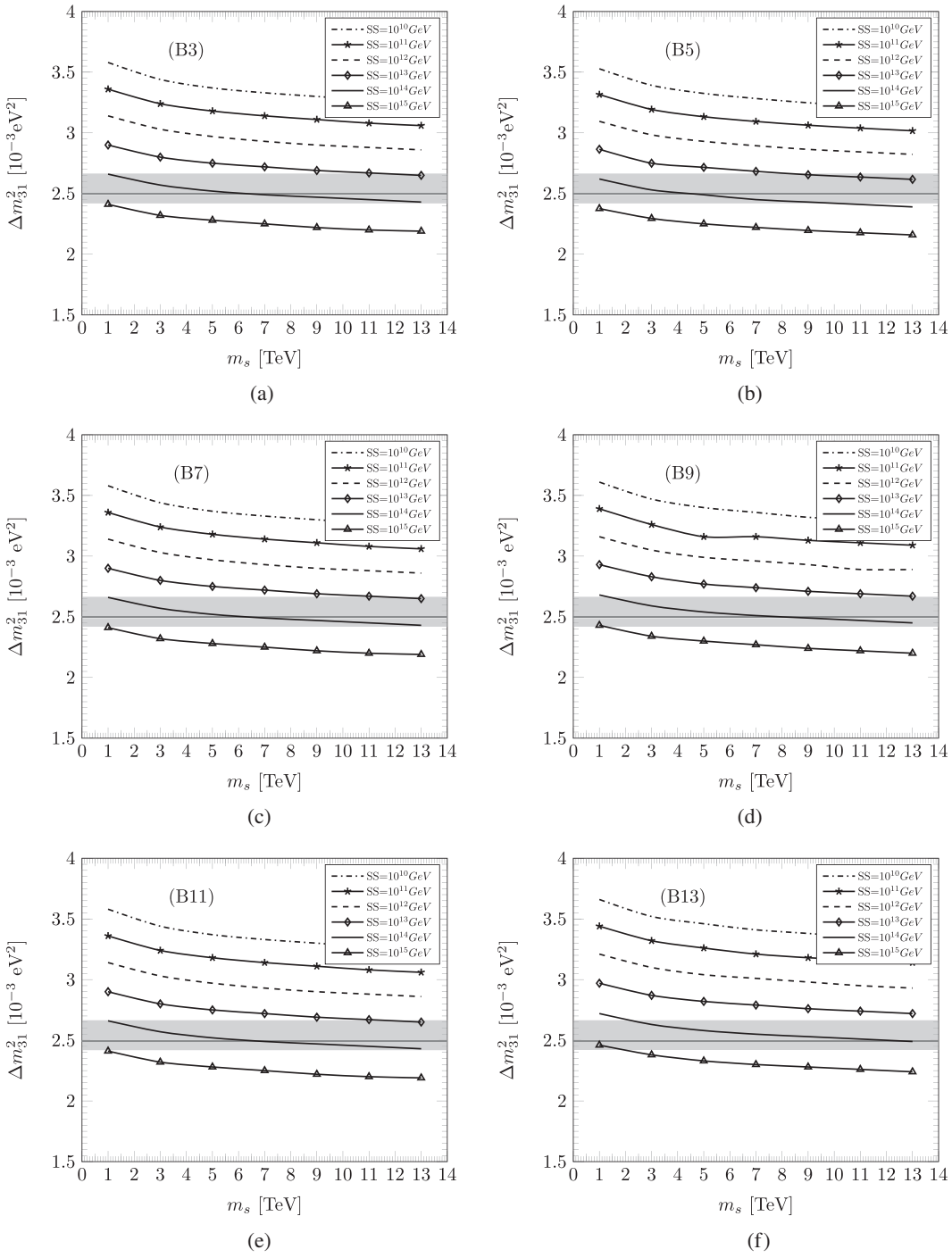

FIG. 7. The fluctuations of the numerical values of Δm^2_{31}, at the EW scale is studied, against changing m_s, and the SS scale. The shaded region (horizontal) represents the experimental 3σ range [1], and the horizontal bold line inside the shaded region indicates the best-fit value. The vertical shaded region corresponds to the allowed m_s region, for which the plots for different SS scale lie within the 3σ bound. The six figures (a), (b), (c), (d), (e), and (f) are for the different input data sets B3, B5, B7, B9, B11, and B13 respectively (as given in Table III). The SS scales are fixed at 10^{10} GeV, 10^{11} GeV, 10^{12} GeV, 10^{13} GeV, 10^{14} GeV, and 10^{15} GeV.

C. The SC relation and the mass ratios

In addition to the physical observables, we try to see how the certain parameters/relation evolve against the varying energy scale. Although the neutrino oscillation experiments hints not for individual neutrino masses, yet the study of individual parameters and how they evolve carry physical insight. This study is relevant from the model building point of view.

(a) As stated earlier, we have assumed that at the SS scale, the three mixing angles are connected via a comple-

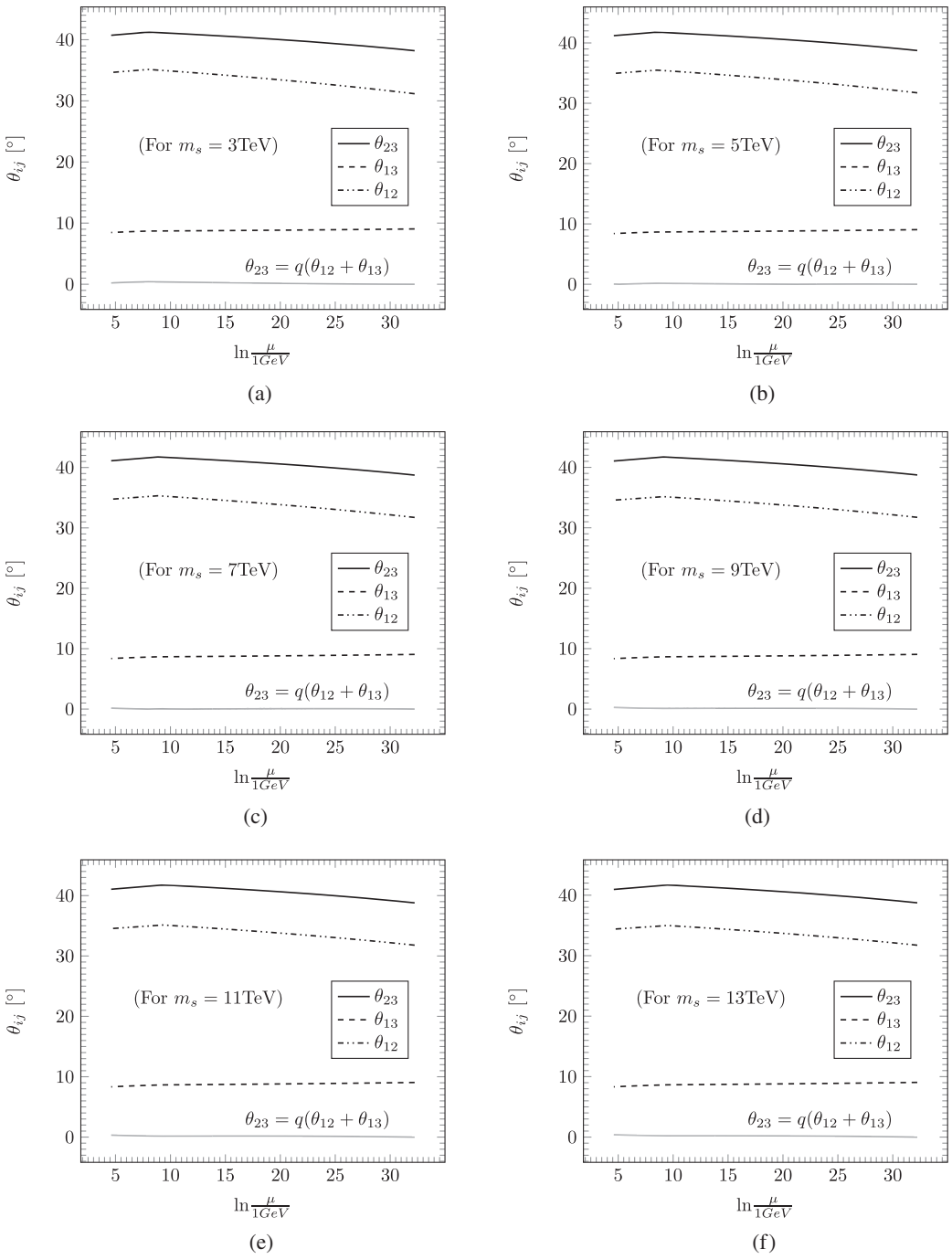

FIG. 8. Radiative evolution of the three neutrino mixing angles and its self-complementarity relation from the seesaw scale to the EW scale for different choices of m_s are studied. The six figures (a), (b), (c), (d), (e), and (f) are for the different input data sets B3, B5, B7, B9, B11, and B13 respectively (as given in Table III). Here we consider only one SS scale (10^{14} GeV).

mentarity relation [see Eq. (2)]. We see that for a fixed m_s and a chosen SS scale, with all the input parameters fixed to a certain data set (say, B5), the angles evolve (except θ_{13} which is almost stable), but the SC relation connecting the mixing angles remains almost invariant against the radiative evolution. This stability is achievable, even if we vary the SS scale or m_s. We have shown the radiative evolution of the angles along with the SC relation for both varying m_s (with a fixed SS scale) and varying SS scale (with a fixed m_s). For details, see Figs. 8–9. The SC relation is a phenomenologically motivated relation like the QLC relation [56] that connects the quark and lepton sectors. A relation of this kind bears the signature of a certain hidden symmetry. As pointed out in our analysis, that which reflects the invariance of the former against

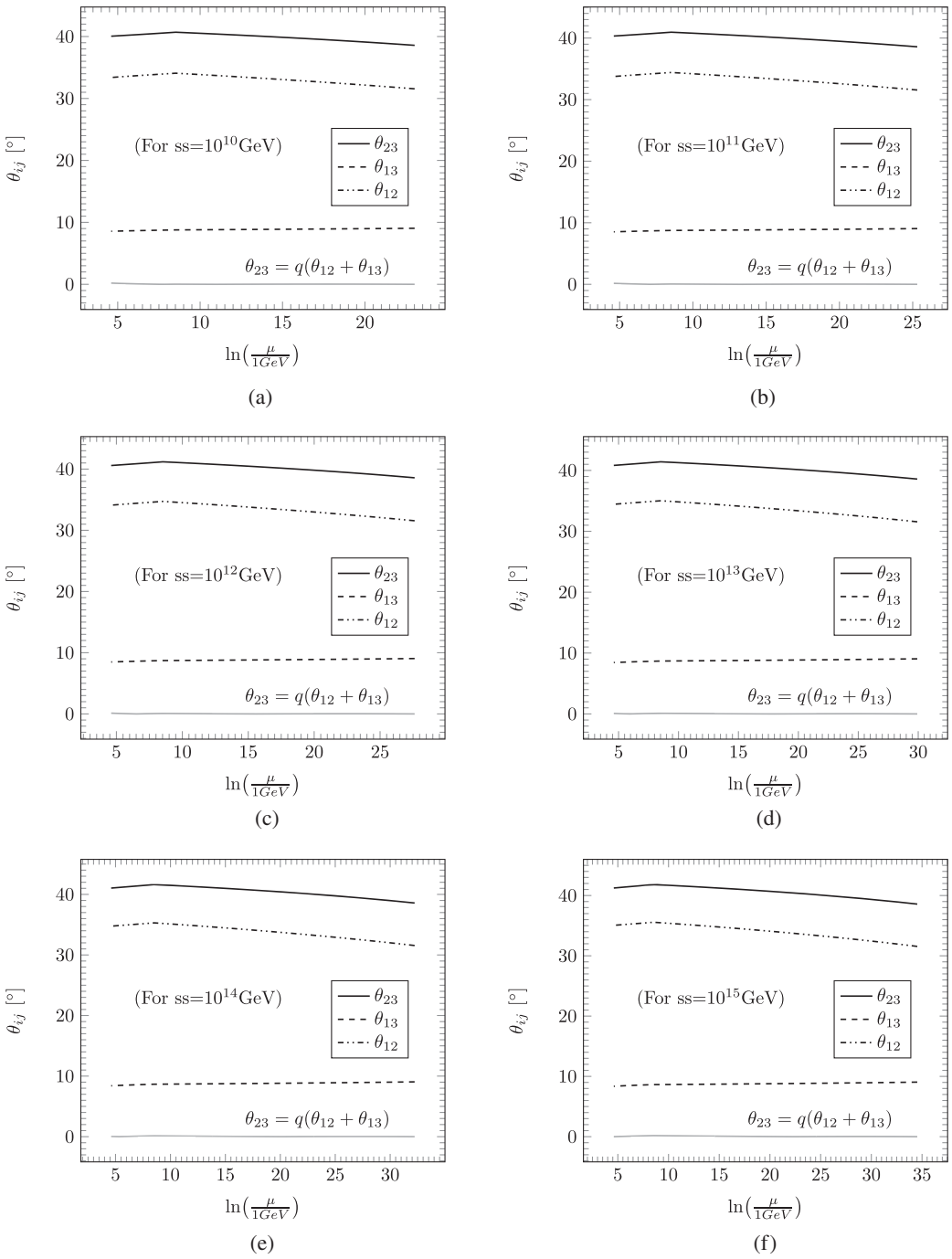

FIG. 9. Radiative evolution of the three neutrino mixing angles and its self-complementarity relation from the seesaw scale to the EW scale for a fixed data set B5, $m_s = 5$ TeV (as given in Table III) are studied for different seesaw scales. The six figures (a), (b), (c), (d), (e), and (f) corresponds to the different choices of SS at 10^{10} GeV, 10^{11} GeV, 10^{12} GeV, 10^{13} GeV, 10^{14} GeV, and 10^{15} GeV respectively.

radiative evolution may turn out as fruitful information for the model builders.

(b) Like the mixing angles, we try to see how the mass parameters respond to radiative evolution. Instead of concentrating on individual neutrino masses, we focus on the three mass ratios as such: m_2/m_1, m_3/m_1, and m_3/m_2. This is inspired by the phenomenology of the quark sector. Where we see that the mass ratio between the down and strange quarks is naturally related to the quark mixing angle (Cabibbo angle) which plays an important role in describing the mixing among the quarks [57,58]. To exemplify, we fix the m_s at 5 TeV and the input data set at $B5$. Following this, we see how the three neutrino mass ratios vary against the changing SS scale. The details are shown in Fig. 10. One sees that the ratio m_3/m_1 or

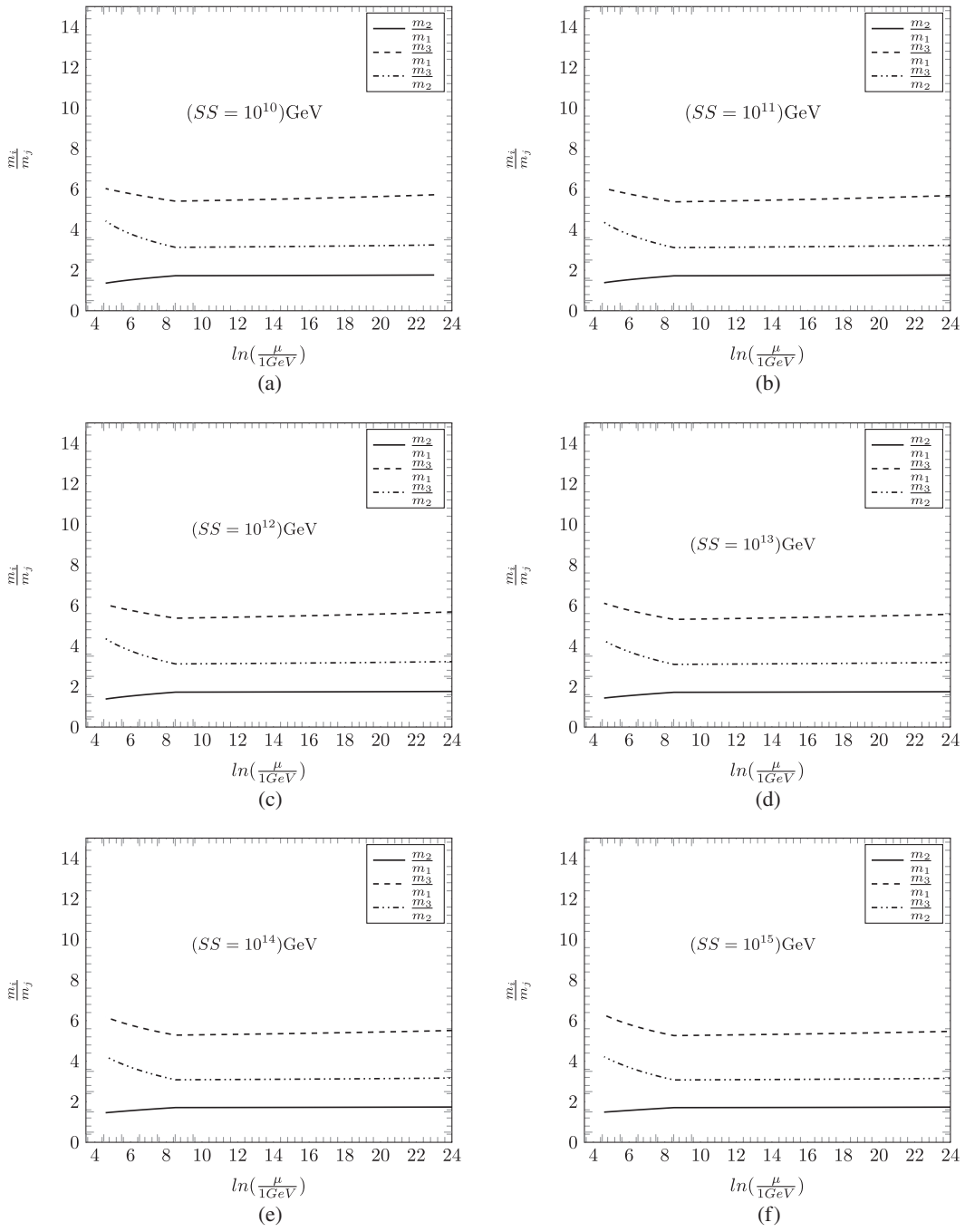

FIG. 10. Radiative evolution of the three neutrino mass ratios from the seesaw scale to the EW scale for a fix input data set B5, fix $m_s = 5$ TeV (as given in Table III) for different seesaw scales are studied. The six figures (a), (b), (c), (d), (e), and (f) corresponds to the different choices of SS at 10^{10} GeV, 10^{11} GeV, 10^{12} GeV, 10^{13} GeV, 10^{14} GeV, and 10^{15} GeV respectively.

m_3/m_2, though remains invariant in the SUSY region, changes after crossing the m_s scale. But, interestingly, the ratio m_2/m_1 remains almost invariant and tries to maintain a constant numerical value as such: $m_2/m_1 \sim 2$. A summarized version of the different types of effect each neutrino parameters receive due to the variation of m_s and SS are given in Table XII.

V. SUMMARY AND DISCUSSION

In this paper, we have studied the radiative evolution of neutrino observational parameters for varying m_s scale following a top-down approach. We presume the hierarchy of the three neutrino masses to be of a normal type. All the nine observational parameters related to neutrino oscillations are allowed to run down from the seesaw scale up to the electroweak scale using their respective RGEs (both

MSSM and SM). We also use the RGEs of the three gauge couplings, third generation Yukawa couplings, and quartic Higgs coupling. All the neutrino parameters along with the other couplings undergo RG evolution and subsequently, get different RG corrections. The m_s, which appears to be a leading parameter, is kept varying between 1 TeV to 13 TeV, and the effect of such a variation on the observational parameters at the EW scale is noted. Instead of adhering to a fixed SS scale, we allow the latter to change between 10^{10} GeV to 10^{15} GeV and have checked how the observational parameters vary. Besides, the work reveals that the self-complementarity relation among the mixing angles remains stable against the radiative evolution. Also, we have studied how certain parameters like neutrino mass ratios behave during this evolution.

The relevance of the SUSY is unavoidable in the context of particle physics, as it can answer to certain important theoretical issues like the hierarchy problem, the unification of gauge couplings, the existence of dark matter etc. But, unlike the Standard Model, the SUSY is still lacking the experimental evidences. Although the LHC experiment is running at 13 TeV, it has not yet witnessed any signature of SUSY. This may imply that the SUSY breaks at a certain higher energy scale which is not yet achieved by the LHC experiment, or even if it breaks at a low energy, the beam luminosity available in the LHC experiment is not sufficient to detect the same. Hence, there is still a hope that SUSY exists. The SUSY breaking scale, m_s, is an important parameter and influences the neutrino observational parameters. The origin of a neutrino mass owes to the seesaw mechanism, and the scale at which the latter occurred is also unknown. But theoretically one may predict that scale to be lying within the range of 10^{10} to 10^{15} GeV. In our analysis, these two parameters, the m_s and the SS scale, partake a lot. Besides, the input data set (like, Aj or Bj) which are although model independent, plays an important role. Initially, the input parameters in the data sets are chosen such that against a fixed m_s and a fixed SS scale (10^{14} GeV), the neutrino observational parameters at the EW scale lie within the 3σ bound. It is mentioned that the initial entries in terms of the three mixing angles follow a self-complementarity relation.

At the EW scale, the three mixing angles, CP violating phases, and Δm^2_{31} try to maintain more or less stability with respect to the 3σ bound if the m_s scale is varied at a fixed SS scale. But the parameter Δm^2_{21} is less stable at lower m_s, whereas the stability increases towards higher m_s. Similar stability is achievable for the three mixing angles if the SS scale is varied. But for Δm^2_{31}, the stability is lost. One sees that if the stability of Δm^2_{21} is obtained towards a higher m_s, ruling out of a certain SS scale is possible in the light of a 3σ bound of Δm^2_{21}. It is worth mentioning that a strong conclusion in view of the optimization of the SUSY breaking and SS scales can not be drawn by observing the plots [see Figs. 6–7], because the Δm^2_{21} at the EW scale is very much sensitive to the initial arbitrary model independent entries available in the data sets (Aj and Bj). Justifying these initial entries under a certain model or framework goes beyond the scope of this article. But through our analysis, one can at least visualize the interplay between the m_s and the SS scale and how these affects the final physical observables. Though in the present analysis, we limit ourselves not to invoke the model dependent ground of these data sets, yet we emphasize the certain traits that these numerals may carry. We see that the data set are characterized by the SC relation, $\theta_{13} + \theta_{12} \approx \theta_{23}$ and a mass ratio: $m_2/m_1 \sim 2$, which remains almost invariant against radiative evolution. Besides, we have observed the other mass ratios like m_3/m_1 or m_3/m_2 also try to maintain a stability up to the SUSY breaking scale, but after that they change. This study is motivated in the context of the quark sector, where the quark mass ratio $m_{\text{down}}/m_{\text{strange}}$ plays an important role in describing the quark mixing. Relations among certain parameters and their stability during radiative evolution may bear the traits of a certain hidden symmetry present in the lepton sector and may serve as a key to some new models.

The present study is devoted to a simple visualization, concerning the interplay between the m_s and SS scale and its effect on the physical observables and certain phenomenological relations. The two Majorana phases are not yet been measured experimentally, and to simplify the analysis, we have considered both of them as equal. Again, we have restricted ourselves only to the normal hierarchy of neutrino masses. The consideration of a degenerate spectrum for all sparticles that we have adopted in our work is an idealized situation and is true if $m_s \gg m_t, m_Z$ [59,60]. In principle, a general study can be made by minimizing the number of assumptions in order to get a more generalized result.

ACKNOWLEDGMENTS

K. S. S would like to thank UGC for their financial support (Grant No. F.7-65/2007(BSR)).

APPENDIX A: RENORMALIZATION GROUP EQUATIONS

1. RGEs for gauge couplings

The two loop renormalization group equations for gauge couplings are [61–63] as follows:

$$\frac{dg_i}{dt} = \frac{b_i}{16\pi^2} g_i^3 + \left(\frac{1}{16\pi^2}\right)^2 \left[\sum_{j=1}^{3} b_{ij} g_i^3 g_j^2 - \sum_{j=t,b,\tau} a_{ij} g_i^3 h_j^2\right], \tag{A1}$$

where, $t = ln\mu$ and b_i, b_{ij}, a_{ij} are β function coefficients in MSSM,

$$b_i = (6.6, 1.0, -3.0), \qquad b_{ij} = \begin{pmatrix} 7.96 & 5.40 & 17.60 \\ 1.80 & 25.00 & 24.00 \\ 2.20 & 9.00 & 14.00 \end{pmatrix}, \qquad a_{ij} = \begin{pmatrix} 5.2 & 2.8 & 3.6 \\ 6.0 & 6.0 & 2.0 \\ 4.0 & 4.0 & 0.0 \end{pmatrix},$$

and, for the nonsupersymmetric case, we have

$$b_i = (4.100, -3.167, -7.000), \qquad g_{ij} = \begin{pmatrix} 3.98 & 2.70 & 8.8 \\ 0.90 & 5.83 & 12.0 \\ 1.10 & 4.50 & -26.0 \end{pmatrix}, \qquad a_{ij} = \begin{pmatrix} 0.85 & 0.5 & 0.5 \\ 1.50 & 1.5 & 0.5 \\ 2.00 & 2.0 & 0.0 \end{pmatrix}.$$

2. RGEs for Yukawa couplings

At two-loop level for MSSM, [61–63]

$$\begin{aligned}
\frac{dh_t}{dt} &= \frac{h_t}{16\pi^2}\left(6h_t^2 + h_b^2 - \sum_{i=1}^{3} c_i g_i^2\right) \\
&\quad + \frac{h_t}{(16\pi^2)^2}\left[\sum_{i=1}\left(c_i b_i + \frac{c_i^2}{2}\right) g_i^4 + g_1^2 g_2^2 + \frac{136}{45} g_1^2 g_3^2 + 8 g_2^2 g_3^2 + \left(\frac{6}{5} g_1^2 + 6 g_2^2 + 16 g_3^2\right) h_t^2\right. \\
&\qquad \left. + \frac{2}{5} g_1^2 h_b^2 - 22 h_t^4 - 5 h_b^4 - 5 h_t^2 h_b^2 - h_b^2 h_\tau^2\right], \\
\frac{dh_b}{dt} &= \frac{h_b}{16\pi^2}\left(6h_b^2 + h_\tau^2 + h_t^2 - \sum_{i=1}^{3} c_i' g_i^2\right) \\
&\quad + \frac{h_b}{(16\pi^2)^2}\left[\sum_{i=1}\left(c_i' b_i + \frac{c_i'^2}{2}\right) g_i^4 + g_1^2 g_2^2 + \frac{8}{9} g_1^2 g_3^2 + 8 g_2^2 g_3^2 + \left(\frac{2}{5} g_1^2 + 6 g_2^2 + 16 g_3^2\right) h_b^2\right. \\
&\qquad \left. + \frac{4}{5} g_1^2 h_\tau^2 + \frac{6}{5} g_1^2 h_\tau^2 - 22 h_b^4 - 3 h_\tau^4 - 5 h_t^4 - 5 h_b^2 h_t^2 - 3 h_b^2 h_\tau^2\right], \\
\frac{dh_\tau}{dt} &= \frac{h_\tau}{16\pi^2}\left(4h_\tau^2 + 3h_b^2 - \sum_{i=1}^{3} c_i'' g_i^2\right) \\
&\quad + \frac{h_\tau}{(16\pi^2)^2}\left[\sum_{i=1}\left(c_i'' b_i + \frac{c_i''^2}{2}\right) g_i^4 + \frac{9}{5} g_1^2 g_2^2 + \left(\frac{6}{5} g_1^2 + 6 g_2^2\right) h_\tau^2\right. \\
&\qquad \left. + \left(\frac{-2}{5} g_1^2 + 16 g_3^2\right) h_b^2 + 9 h_b^4 - 10 h_\tau^4 - 3 h_b^2 h_t^2 - 9 h_b^2 h_\tau^2\right],
\end{aligned} \tag{A2}$$

where

$$c_i = \left(\frac{13}{15}, 3, \frac{16}{13}\right), \qquad c_i' = \left(\frac{7}{15}, 3, \frac{16}{3}\right), \qquad c_i'' = \left(\frac{9}{5}, 3, 0\right).$$

Yukawa RGEs for the nonsupersymmetric case,

$$\begin{aligned}
\frac{dh_t}{dt} &= \frac{h_t}{16\pi^2}\left(\frac{3}{2}h_t^2 - \frac{3}{2}h_b^2 + Y_2(S) - \sum_{i=1}^{3} c_i g_i^2\right) \\
&+ \frac{h_t}{(16\pi^2)^2}\left[\frac{1187}{600}g_1^4 - \frac{23}{4}g_2^4 - 108g_3^4 - \frac{9}{20}g_1^2g_2^2 + \frac{19}{15}g_1^2g_3^2 + 9g_2^2g_3^2 + \left(\frac{223}{80}g_1^2 + \frac{135}{16}g_2^2 + 16g_3^2\right)h_t^2\right. \\
&\quad - \left(\frac{43}{80}g_1^2 - \frac{9}{16}g_2^2 + 16g_3^2\right)h_b^2 + \frac{5}{2}Y_4(S) - 2\lambda(3h_t^2 + h_b^2) + \frac{3}{2}h_t^4 - \frac{5}{4}h_t^2h_b^2 + \frac{11}{4}h_b^4 \\
&\quad \left. + Y_2(S)\left(\frac{5}{4}h_b^2 - \frac{9}{4}h_t^2\right) - \chi_4(S) + \frac{3}{2}\lambda^2\right], \\
\frac{dh_b}{dt} &= \frac{h_b}{16\pi^2}\left(\frac{3}{2}h_b^2 - \frac{3}{2}h_t^2 + Y_2(S) - \sum_{i=1}^{3} c_i' g_i^2\right) \\
&+ \frac{h_b}{(16\pi^2)^2}\left[-\frac{127}{600}g_1^4 - \frac{23}{4}g_2^4 - 108g_3^4 - \frac{27}{20}g_1^2g_2^2 + \frac{31}{15}g_1^2g_3^2 + 9g_2^2g_3^2 - \left(\frac{79}{80}g_1^2 - \frac{9}{16}g_2^2 + 16g_3^2\right)h_t^2\right. \\
&\quad + \left(\frac{187}{80}g_1^2 + \frac{135}{16}g_2^2 + 16g_3^2\right)h_b^2 + \frac{5}{2}Y_4(S) - 2\lambda(h_t^2 + 3h_b^2) + \frac{3}{2}h_b^4 - \frac{5}{4}h_t^2h_b^2 \\
&\quad \left. + \frac{11}{4}h_t^4 + Y_2(S)\left(\frac{5}{4}h_t^2 - \frac{9}{4}h_b^2\right) - \chi_4(S) + \frac{3}{2}\lambda^2\right], \\
\frac{dh_\tau}{dt} &= \frac{h_\tau}{16\pi^2}\left(\frac{3}{2}h_\tau^2 + Y_2(S) - \sum_{i=1}^{3} c_i'' g_i^2\right) \\
&+ \frac{h_\tau}{(16\pi^2)^2}\left[\frac{1371}{200}g_1^4 - \frac{23}{4}g_2^4 - \frac{27}{20}g_1^2g_2^2 + \left(\frac{387}{80}g_1^2 + \frac{135}{16}g_2^2\right)h_\tau^2 + \frac{5}{2}Y_4(S) - 6\lambda h_t^2 + \frac{3}{2}h_\tau^4 - \frac{9}{4}Y_2(S)h_\tau^2 - \chi_4(S) + \frac{3}{2}\lambda^2\right],
\end{aligned} \tag{A3}$$

$$\begin{aligned}
\frac{d\lambda}{dt} &= \frac{1}{16\pi^2}\left[\frac{9}{4}\left(\frac{3}{25}g_1^4 + \frac{2}{5}g_1^2g_2^2 + g_2^4\right) - \left(\frac{9}{5}g_1^2 + 9g_2^2\right)\lambda + 4Y_2(S)\lambda - 4H(S) + 12\lambda^2\right] \\
&+ \frac{1}{(16\pi^2)^2}\left[-78\lambda^3 + 18\left(\frac{3}{5}g_1^2 + 3g_2^2\right)\lambda^2 + \left(-\frac{73}{8}g_2^4 + \frac{117}{20}g_1^2g_2^2 + \frac{1887}{200}g_1^4\right)\lambda + \frac{305}{8}g_2^6 - \frac{867}{120}g_1^2g_2^4 - \frac{1677}{200}g_1^4g_2^2\right. \\
&\quad - \frac{3411}{1000}g_1^6 - 64g_3^2(h_t^4 + h_b^4) - \frac{8}{5}g_1^2(2h_t^4 - h_b^4 + 3h_\tau^4) - \frac{3}{2}g_2^4Y_2(S) + 10\lambda Y_4(S) \\
&\quad + \frac{3}{5}g_1^2\left(-\frac{57}{10}g_1^2 + 21g_2^2\right)h_t^2 + \left(\frac{3}{2}g_1^2 + 9g_2^2\right)h_b^2 + \left(-\frac{15}{2}g_1^2 + 11g_2^2\right)h_\tau^2 - 24\lambda^2Y_2(S) - \lambda H(S) \\
&\quad \left. + 6\lambda h_t^2h_b^2 + 20(3h_t^6 + 3h_b^6 + h_\tau^6) - 12(h_t^4h_b^2 + h_t^2h_b^4)\right],
\end{aligned} \tag{A4}$$

where

$$\begin{aligned}
Y_2(S) &= 3h_t^2 + 3h_b^2 + h_\tau^2, \\
Y_4(S) &= \frac{1}{3}\left[3\sum c_i g_i^2 h_t^2 + 3\sum c_i' g_i^2 h_b^2 + 3\sum c_i'' g_i^2 h_\tau^2\right], \\
\chi_4(S) &= \frac{9}{4}\left[3h_t^4 + 3h_b^4 + h_\tau^4 - \frac{2}{3}h_t^2h_b^2\right], \\
H(S) &= 3h_t^4 + 3h_t^4 + h_\tau^4, \\
\lambda &= \frac{m_h^2}{V^2}, \quad \text{is the Higgs self coupling } (m_h = \text{Higgs mass}),
\end{aligned} \tag{A5}$$

with the values of beta function coefficients for non-SUSY case and

$$c_i = (0.85, 2.25, 8.00), \qquad c_i' = (0.25, 2.25, 8.00), \qquad c_i'' = (2.25, 2.25, 0.00).$$

3. Tables

TABLE II. The initial values of the neutrino parameters [$(\theta_{ij})_0$ and $(m_i)_0$] against varying Majorana phase [$(\psi_1)_0$, $(\psi_2)_0$, with, $(\psi_1)_0 = (\psi_2)_0$]. The m_s and the SS scale are fixed at 5 TeV and 10^{14} GeV, respectively. We choose, the initial value of the Dirac phase, $(\delta)_0 = 90°$, and $(m_2)_0 = 2.340 \times 10^{-2}$ eV. The purpose of this study is to achieve the numerical values of the parameters within 3σ range at EW scale.

$(\psi_1)_0/° \rightarrow$	0.0	45	90	135	180	225	270	315	360
$(\theta_{23})_0/° \rightarrow$	37.240	37.240	37.240	37.240	37.240	37.240	37.240	37.240	37.240
$(\theta_{12})_0/° \rightarrow$	29.160	29.160	29.160	29.160	29.160	29.160	29.160	29.160	29.160
$(\theta_{13})_0/° \rightarrow$	7.974	7.974	7.974	7.974	7.974	7.974	7.974	7.974	7.974
$(m_1)_0 \times 10^{-2}$ eV $\rightarrow$	1.370	1.375	1.380	1.390	1.395	1.389	1.380	1.375	1.370
$(m_3)_0 \times 10^{-2}$ eV $\rightarrow$	7.791	7.802	7.626	7.460	7.470	7.469	7.522	7.801	7.779

TABLE III. The table for different sets of input parameters to be used for subsequent analysis. The $(\theta_{23})_0$ is connected to $(\theta_{13})_0$ and $(\theta_{12})_0$ via the S.C relation as presumed in Eq. (2). We choose only the $(\theta_{13})_0$ and $(\theta_{12})_0$ as input. The Majorana phase $(\psi_1)_0$ is fixed at 45°. The sets $A1, A3, ...A13$ represent the collection of initial inputs to be attributed to the parameters at the SS scale, for the m_s scale being fixed at $1, 3…13$ TeV, respectively, with $(\delta)_0 = 90°$. The SS scale is fixed at 10^{14} GeV. The sets $B1, B2, …B13$ are similar to the sets $A1, A3…A13$, respectively, except for the former, $(\delta)_0 = 270°$. The numerical entries are adjusted for a specific m_s scale (say, $A5$ at 5 TeV) so that after running the RGEs, the parameters at the EW scale lie within the 3σ range.

	Different possible sets of neutrino parameters input values at the seesaw scale													
	↓	↓	↓	↓	↓	↓	↓	↓	↓	↓	↓	↓	↓	↓
Input ν parameters	$A1$	$A3$	$A5$	$A7$	$A9$	$A11$	$A13$	$B1$	$B3$	$B5$	$B7$	$B9$	$B11$	$B13$
$(m_1)_0$	1.51	1.36	1.32	1.29	1.27	1.25	1.23	1.51	1.38	1.33	1.30	1.27	1.25	1.24
$(m_2)_0$	2.34	2.34	2.34	2.34	2.34	2.34	2.34	2.34	2.34	2.34	2.34	2.34	2.34	2.34
$(m_3)_0$	7.61	7.74	7.79	7.81	7.86	7.92	7.92	7.46	7.56	7.58	7.63	7.65	7.68	7.72
$(\theta_{12})_0/°$	30.36	31.05	31.45	31.46	31.51	31.62	31.79	30.36	31.22	31.79	31.79	31.79	31.79	31.79
$(\theta_{13})_0/°$	8.42	8.53	8.53	8.53	8.53	8.53	8.53	8.93	9.05	9.05	9.05	9.05	9.05	9.05
$(\theta_{23})_0/°$	37.12	37.61	37.99	37.99	38.04	38.15	38.31	38.12	38.26	38.80	38.80	38.80	38.80	38.80
q	0.96	0.95	0.95	0.95	0.95	0.95	0.95	0.97	0.95	0.95	0.95	0.95	0.95	0.95
$(\psi_1)_0/°$	45.0	45.0	45.0	45.0	45.0	45.0	45.0	45.0	45.0	45.0	45.0	45.0	45.0	45.0
$(\delta)_0/°$	90.0	90.0	90.0	90.0	90.0	90.0	90.0	270.0	270.0	270.0	270.0	270.0	270.0	270.0

TABLE IV. The fluctuations of a solar mass squared difference after RG evolution at the EW scale have been studied against a changing m_s at a constant SS scale. The Aj or Bj correspond to the set of initial entries at constant m_s as mentioned in Table III. The diagonal entries marked in bold text reflect the output values of, Δm^2_{21} within 3σ for which the initial entries of Aj or Bj were tuned at constant m_s. On keeping a input data set (say, $A5$) fixed, if the m_s scale is varied, one sees that, against the radiative correction, the value of Δm^2_{21} at the EW scale fluctuates. If m_s is lesser, the fluctuation is more. The output values which lies within 3σ are underlined. The irrelevant output are omitted with an "×" sign.

	$\Delta m^2_{12}(\times 10^{-5}$ eV$^2)$ at EW scale													
m_s in TeV	$A1$	$A3$	$A5$	$A7$	$A9$	$A11$	$A13$	$B1$	$B3$	$B5$	$B7$	$B9$	$B11$	$B13$
1.0	**7.56**	11.11	13.00	12.98	13.50	13.86	14.19	**7.56**	11.08	12.34	13.01	13.52	13.89	14.21
3.0	1.79	**7.56**	9.16	9.82	10.81	10.89	11.25	1.88	**7.57**	9.05	9.63	10.42	10.84	11.20
5.0	×	5.94	**7.57**	8.42	9.06	9.47	9.844	×	5.95	**7.58**	8.43	9.06	9.50	9.88
7.00	×	4.87	6.64	**7.55**	8.21	8.64	9.01	×	4.87	6.64	**7.55**	8.20	8.66	9.06
9.0	×	4.01	5.93	6.89	**7.57**	8.01	8.400	×	4.00	5.93	6.88	**7.56**	8.03	8.44
11.0	×	3.30	5.39	6.38	7.08	**7.54**	7.92	×	3.27	5.37	6.36	7.07	**7.56**	7.97
13.0	×	2.64	4.919	5.95	6.675	7.13	**7.53**	×	2.61	4.89	5.29	6.65	7.15	**7.55**

TABLE V. The fluctuations of the atmospheric mass squared difference after RG evolution, at the EW scale have been studied, against changing m_s, at a constant SS scale. The Aj or Bj correspond to the set of initial entries at a constant m_s as mentioned in Table III. The diagonal entries marked in bold text reflect the output values of Δm^2_{31} within 3σ for which the initial entries of Aj or Bj were tuned at a constant m_s. On keeping a input data set (say, $A5$) fixed, if the m_s scale is varied, one sees that, against the radiative correction, the value of Δm^2_{31} at the EW scale fluctuates. If m_s is lesser, the fluctuation is more. The output values which lies within 3σ are underlined. The irrelevant results in view of 3σ bound are omitted with an "×" symbol.

	$\Delta m^2_{23}(\times 10^{-3}\ \mathrm{eV}^2)$ at EW scale for different sets of inputs													
m_s in TeV	$A1$	$A3$	$A5$	$A7$	$A9$	$A11$	$A13$	$B1$	$B3$	$B5$	$B7$	$B9$	$B11$	$B13$
1.0	**2.51**	2.65	2.86	2.703	2.74	2.80	2.80	**2.49**	2.59	2.62	2.66	2.68	2.71	2.74
3.0	2.40	**2.53**	2.62	2.57	2.62	2.67	2.67	2.40	**2.50**	2.53	2.53	2.59	2.62	2.64
5.0	×	2.48	**2.51**	2.51	2.56	2.61	2.61	×	2.45	**2.49**	2.52	2.54	2.57	2.60
7.0	×	2.44	2.47	**2.48**	2.52	2.57	2.57	×	2.42	2.45	**2.49**	2.51	2.54	2.56
9.0	×	2.41	2.44	2.44	**2.49**	2.54	2.54	×	2.40	2.43	2.47	**2.48**	2.51	2.53
11.0	×	2.39	2.41	2.42	2.46	**2.51**	2.51	×	2.38	2.41	2.45	2.46	**2.49**	2.52
13.0	×	2.37	2.39	2.40	2.44	2.49	**2.44**	×	2.36	2.39	2.43	2.45	2.47	**2.49**

TABLE VI. The fluctuations of an atmospheric angle after RG evolution, at the EW scale have been studied, against changing m_s, at a constant SS scale. The Aj or Bj represent the set of initial entries at a constant m_s as mentioned in Table III. The diagonal entries marked in bold text reflect the output values of, θ_{23} within 3σ for which the initial entries of Aj or Bj are adjusted at constant m_s. On keeping a input data set (say, $A5$) fixed, if the m_s scale is varied, one sees that, against the radiative correction, the value of θ_{23} at the EW scale fluctuates, but a little and output values lie within 3σ range. The irrelevant results in view of 3σ bound are omitted with an "×" symbol.

	$\theta_{23}/^\circ$ at EW scale													
m_s in TeV	$A1$	$A3$	$A5$	$A7$	$A9$	$A11$	$A13$	$B1$	$B3$	$B5$	$B7$	$B9$	$B11$	$B13$
1.0	**41.0**	41.4	41.6	41.8	41.8	41.9	42.1	**41.0**	41.1	41.6	41.6	41.6	41.6	41.6
3.0	40.6	**41.1**	41.4	41.5	41.5	41.6	41.8	40.7	**40.8**	41.3	41.3	41.3	41.3	41.3
5.0	×	41.0	**41.3**	41.3	41.4	41.5	41.6	×	40.7	**41.2**	41.2	41.2	41.2	41.2
7.0	×	40.9	41.2	**41.2**	41.3	41.4	41.5	×	40.6	41.1	**41.1**	41.1	41.1	41.1
9.0	×	40.8	41.2	41.2	**41.2**	41.3	41.4	×	40.5	41.1	41.1	**41.1**	41.0	41.0
11.0	×	40.8	41.1	41.1	41.1	**41.2**	41.4	×	40.5	41.0	41.0	41.0	**41.0**	41.0
13.0	×	40.7	41.1	41.0	41.1	41.2	**41.3**	×	40.4	41.0	41.0	41.0	41.0	**41.0**

TABLE VII. The fluctuation of a solar angle after RG evolution, at the EW scale is studied, against changing m_s, at a constant SS scale. The Aj or Bj represent the set of initial entries at a constant m_s as mentioned in Table III. The diagonal entries marked in bold texts reflect the output values of, θ_{12} within 3σ for which the initial entries of Aj or Bj are adjusted at constant m_s. On keeping a input data set (say, $A5$) fixed, if the m_s scale is varied, one sees that, against the radiative correction, the value of θ_{12} at the EW scale fluctuates, but the variations are little and the output values lie within 3σ range.

	$\theta_{12}/^\circ$ at EW scale													
m_s in TeV	$A1$	$A3$	$A5$	$A7$	$A9$	$A11$	$A13$	$B1$	$B3$	$B5$	$B7$	$B9$	$B11$	$B13$
1.0	**34.6**	34.8	34.8	34.8	34.8	34.8	35.0	**34.8**	35.0	35.3	35.1	35.1	35.1	35.0
3.0	34.1	**34.4**	34.6	34.6	34.5	34.6	34.7	34.3	**34.7**	35.0	34.9	34.9	34.8	34.7
5.0	×	34.3	**34.5**	34.4	34.4	34.5	34.6	×	34.5	**34.9**	34.7	34.7	34.7	34.6
7.0	×	34.2	34.4	**34.3**	34.3	34.4	34.5	×	34.4	34.8	**34.6**	34.7	34.6	34.5
9.0	×	34.1	34.4	34.3	**34.2**	34.3	34.5	×	34.3	34.7	34.6	**34.6**	34.5	34.5
11.0	×	34.0	34.3	34.2	34.2	**34.3**	34.4	×	34.3	34.6	34.5	34.5	**34.5**	34.48
13.0	×	34.0	34.3	34.2	34.2	34.2	**34.4**	×	34.2	34.6	34.5	34.5	34.4	**34.4**

TABLE VIII. The fluctuation of the reactor angle after RG evolution at the EW scale is investigated, against changing m_s, at a constant SS scale. The Aj or Bj represent the set of initial entries at a constant m_s as mentioned in Table III. The diagonal entries marked in bold texts represent the output values of, θ_{23} within 3σ for which the initial entries of Aj or Bj are adjusted at a constant m_s. On keeping an input data set (say, $A5$) fixed, if the m_s scale is varied, one sees that, against the radiative correction, the value of θ_{23} at the EW scale fluctuates. The fluctuation is very feeble against the varying m_s. The irrelevant results in view of 3σ bound are omitted with an "×" symbol.

	$\theta_{13}/^\circ$ at EW													
m_s in TeV	$A1$	$A3$	$A5$	$A7$	$A9$	$A11$	$A13$	$B1$	$B3$	$B5$	$B7$	$B9$	$B11$	$B13$
1.0	**8.4**	8.6	8.6	8.6	8.6	8.6	8.6	**8.4**	8.5	8.4	8.4	8.4	8.4	8.4
3.0	8.4	**8.5**	8.5	8.5	8.5	8.5	8.5	8.3	**8.4**	8.4	8.3	8.4	8.4	8.4
5.0	×	8.4	**8.4**	8.5	8.50	8.50	8.5	×	8.4	**8.3**	8.3	8.3	8.3	8.3
7.0	×	8.4	8.4	**8.4**	8.4	8.4	8.4	×	8.3	8.3	**8.3**	8.3	8.3	8.3
9.0	×	8.4	8.4	8.4	**8.4**	8.4	8.4	×	8.3	8.3	8.3	**8.3**	8.3	8.3
11.0	×	8.4	8.4	8.4	8.4	**8.4**	8.4	×	8.3	8.3	8.3	8.3	**8.3**	8.3
13.0	×	8.4	8.4	8.4	8.4	8.4	**8.4**	×	8.3	8.3	8.3	8.3	8.3	**8.3**

TABLE IX. The fluctuations of m_1 after RG evolution at the EW scale have been studied, against changing m_s, at a constant SS scale. The Aj or Bj correspond to the set of initial entries at a constant m_s as mentioned in Table III. On keeping an input data set (say, $A5$) fixed, if the m_s scale is varied, one sees that, against the radiative correction, the value of m_1 at the EW scale fluctuates. The irrelevant results in view of 3σ bound are omitted with an "×" symbol.

	$m_1 \times 10^{-3}$ eV at EW scale for different sets of inputs													
m_s in TeV	$A1$	$A3$	$A5$	$A7$	$A9$	$A11$	$A13$	$B1$	$B3$	$B5$	$B7$	$B9$	$B11$	$B13$
1.0	10.30	9.43	9.35	8.83	8.66	8.53	8.40	10.29	9.46	9.04	8.83	8.67	8.55	8.44
3.0	9.63	8.82	8.56	8.26	8.10	7.98	7.85	9.62	8.85	8.45	8.06	8.11	8.00	7.89
5.0	×	8.53	8.17	7.99	7.83	7.71	7.59	×	8.56	8.17	7.99	7.84	7.73	7.63
7.0	×	8.34	7.99	7.81	7.65	7.54	7.42	×	8.36	7.99	7.81	7.66	7.56	7.46
9.0	×	8.19	7.84	7.67	7.52	7.40	7.29	×	8.21	7.85	7.67	7.53	7.42	7.33
11.0	×	8.07	7.73	7.56	7.41	7.30	7.18	×	8.10	7.73	7.56	7.42	7.31	7.22
13.0	×	7.97	7.63	7.46	7.31	7.20	7.09	×	7.99	7.63	7.46	7.32	7.22	7.11

TABLE X. The fluctuations of m_2 after RG evolution at the EW scale is studied, against changing m_s, at a constant SS scale. The Aj or Bj correspond to the set of initial entries at a constant m_s as mentioned in Table III. On keeping an input data set (say, $A5$) fixed, if the m_s scale is varied, one sees that, against the radiative correction, the value of m_2 at the EW scale fluctuates. The irrelevant results in view of 3σ bound are omitted with an "×" symbol.

	$m_2 \times 10^{-2}$ eV at EW scale for different sets of inputs													
m_s in TeV	$A1$	$A3$	$A5$	$A7$	$A9$	$A11$	$A13$	$B1$	$B3$	$B5$	$B7$	$B9$	$B11$	$B13$
1.0	1.34	1.41	1.47	1.44	1.44	1.45	1.45	13.47	1.42	1.43	1.44	1.45	1.46	1.46
3.0	1.05	1.23	1.28	1.29	1.30	1.31	1.31	10.55	1.24	1.27	1.27	1.30	1.31	1.32
5.0	×	1.15	1.19	1.21	1.23	1.24	1.24	×	1.15	1.19	1.22	1.23	1.24	1.25
7.0	×	1.08	1.14	1.16	1.18	1.19	1.20	×	1.09	1.14	1.17	1.19	1.20	1.21
9.0	×	1.03	1.09	1.13	1.15	1.16	1.17	×	1.04	1.09	1.13	1.15	1.16	1.18
11.0	×	0.99	1.06	1.10	1.12	1.13	1.14	×	0.99	1.07	1.10	1.12	1.14	1.15
13.0	×	0.95	1.03	1.07	1.09	1.11	1.12	×	0.95	1.04	1.07	1.10	1.11	1.12

TABLE XI. The fluctuations of m_3 after RG evolution at the EW scale is studied, against changing m_s, at a constant SS scale. The Aj or Bj correspond to the set of initial entries at a constant m_s as mentioned in Table III. On keeping an input data set (say, $A5$) fixed, if the m_s scale is varied, one sees that, against the radiative correction, the value of m_3 at the EW scale fluctuates. The irrelevant results in view of 3σ bound are omitted with an "×" symbol.

	$m_3 \times 10^{-2}$ eV at EW scale for different sets of inputs													
m_s in TeV	$A1$	$A3$	$A5$	$A7$	$A9$	$A11$	$A13$	$B1$	$B3$	$B5$	$B7$	$B9$	$B11$	$B13$
1.0	5.12	5.24	5.43	5.27	5.31	5.36	5.36	5.09	5.17	5.20	5.23	5.25	5.27	5.30
3.0	4.99	5.11	5.19	5.14	5.18	5.23	5.23	5.00	5.08	5.10	5.10	5.15	5.18	5.20
5.0	×	5.05	5.07	5.08	5.12	5.17	5.17	×	5.03	5.05	5.09	5.10	5.13	5.15
7.0	×	5.01	5.03	5.04	5.08	5.12	5.12	×	4.99	5.02	5.05	5.07	5.09	5.12
9.0	×	4.98	5.00	5.00	5.04	5.09	5.09	×	4.96	4.99	5.02	5.04	5.07	5.09
11.0	×	4.95	4.97	4.98	5.02	5.06	5.06	×	4.94	4.97	5.00	5.02	5.04	5.07
13.0	×	4.93	4.95	4.95	4.99	5.04	5.04	×	4.92	4.95	4.98	5.00	5.02	5.04

TABLE XII. Here we show the different effects each neutrino parameters receive due to the variation of m_s and SS. An increase in m_s causes a negative effect on all the EW scale neutrino parameters values, except for the Majorana phases (for decreasing m_s the finding is reverse), whereas variation in SS has unequal effects (positive effect on some parameters and negative effects on other parameters). The "−" sign indicates the negative effect, whereas the "+" sign indicate the positive contribution due to varying m_s and SS.

	Effect of varying m_s and SS on the neutrino parameters						
Variation of m_s and SS scale	θ_{12}	θ_{13}	θ_{23}	Δm^2_{21}	Δm^2_{31}	δ	ψ_1
Increasing $m_s \rightarrow$	−	−	−	−	−	−	+
Decreasing $m_s \rightarrow$	+	+	+	+	+	+	−
Increasing SS $\rightarrow$	+	−	+	−	−	+	−
Decreasing SS $\rightarrow$	−	+	−	+	+	−	+

[1] P. F. de Salas, D. V. Forero, C. A. Ternes, M. Tortola, and J. W. F. Valle, arXiv:1708.01186.
[2] M. C. Gonzalez-Garcia, M. Maltoni, and T. Schwetz, Nucl. Phys. **B908**, 199 (2016).
[3] D. V. Naumov, Phys. Part. Nucl. Lett. **8**, 717 (2011).
[4] M. C. Gonzalez-Garcia, *Proc. Sci.*, ICHEP20122013 (2013) 005.
[5] M. Gerbino, M. Lattanzi, and A. Melchiorri, Phys. Rev. D **93**, 033001 (2016).
[6] N. Palanque-Delabrouille *et al.*, J. Cosmol. Astropart. Phys. 02 (2015) 045.
[7] Y. Huang and B.-Q. Ma, The Universe **2**, 65 (2014).
[8] A. Melfo, AIP Conf. Proc. **917**, 252 (2007).
[9] I. Dorsner and P. F. Perez, Nucl. Phys. **B723**, 53 (2005).
[10] E. Dudas, C. Petersson, and P. Tziveloglou, Nucl. Phys. **B870**, 353 (2013).
[11] M. Dine, Nucl. Phys. B, Proc. Suppl. **52A**, 201 (1997).
[12] B. Feldstein and T. T. Yanagida, Phys. Lett. B **720**, 166 (2013).
[13] R. Aaij *et al.* (LHCb Collaboration), Nat. Phys. **11**, 743 (2015).
[14] M. Kazana (CMS Collaboration), Acta Phys. Pol. B **47**, 1489 (2016).
[15] M. Bustamante, A. M. Gago, and J. J. Perez, J. High Energy Phys. 05 (2011) 133.
[16] F. Cadiz and M. A. Daz, Int. J. Mod. Phys. A **29**, 1450158 (2014).
[17] B. Mukhopadhyaya, Proc. Indian Acad. Sci. A **70**, 239 (2004).
[18] K. S. Singh and N. N. Singh, Adv. High Energy Phys. **2015**, 652029 (2015).
[19] G. Apollinari, O. Brüning, T. Nakamoto, and L. Rossi, CERN Yellow Report **5**, 1 (2015).
[20] Technical Report No. CMS-PAS-B2G-17-002, CERN, Geneva, 2017.
[21] M. Aaboud *et al.* (ATLAS Collaboration), arXiv: 1710.07235.
[22] A. V. Gladyshev and D. I. Kazakov, in *Proceedings, 2012 European School of High-Energy Physics (ESHEP 2012): La Pommeraye, Anjou, France, 2012*, p. 107, arXiv: 1212.2548.
[23] S. Demidov, in *Proceedings, CMS Workshop: Perspectives on Physics and on CMS at Very High Luminosity, HL-LHC* (JINR, Dubna, 2013).
[24] Z. Ren and D.-X. Zhang, Eur. Phys. J. Plus **132**, 322 (2017).

[25] C. Arbelaez, M. Hirsch, and L. Reichert, J. High Energy Phys. 02 (2012) 112.
[26] X. Zhang and B.-Q. Ma, Phys. Lett. B **710**, 630 (2012).
[27] N. Haba, K. Kaneta, and R. Takahashi, Europhys. Lett. **101**, 11001 (2013).
[28] H. Minakata and A. Yu. Smirnov, Phys. Rev. D **70**, 073009 (2004).
[29] H. Minakata, in *Eleventh International Workshop on Neutrino Telescopes, Venezia, 2005*, p. 83, arXiv:hep-ph/0505262.
[30] X. Zhang, Y.-j. Zheng, and B.-Q. Ma, Phys. Rev. D **85**, 097301 (2012).
[31] N. Haba and R. Takahashi, J. High Energy Phys. 08 (2013) 123.
[32] R. Foot, A. Kobakhidze, K. McDonald, and R. Volkas, Phys. Rev. D **76**, 075014 (2007).
[33] T. Tsuyuki, Phys. Rev. D **91**, 076004 (2015).
[34] P. F. Harrison, R. Krishnan, and W. G. Scott, Phys. Rev. D **82**, 096004 (2010).
[35] D. A. Demir, J. High Energy Phys. 11 (2005) 003.
[36] V. D. Barger, M. S. Berger, and P. Ohmann, Phys. Rev. D **47**, 1093 (1993).
[37] N. N. Singh and S. B. Singh, Eur. Phys. J. C **5**, 363 (1998).
[38] N. G. Deshpande and E. Keith, Phys. Rev. D **50**, 3513 (1994).
[39] M. K. Parida and N. N. Singh, Phys. Rev. D **59**, 032002 (1998).
[40] Y. Yamada, Z. Phys. C **60**, 83 (1993).
[41] S. Antusch, J. Kersten, M. Lindner, and M. Ratz, Nucl. Phys. **B674**, 401 (2003).
[42] J. A. Casas, J. R. Espinosa, A. Ibarra, and I. Navarro, Nucl. Phys. **B573**, 652 (2000).
[43] W. G. Hollik, Phys. Rev. D **91**, 033001 (2015).
[44] P. H. Chankowski and Z. Pluciennik, Phys. Lett. B **316**, 312 (1993).
[45] K. R. S. Balaji, R. N. Mohapatra, M. K. Parida, and E. A. Paschos, Phys. Rev. D **63**, 113002 (2001).
[46] W. Chao and H. Zhang, Phys. Rev. D **75**, 033003 (2007).
[47] N. Haba, K. Kaneta, R. Takahashi, and Y. Yamaguchi, Nucl. Phys. **B885**, 180 (2014).
[48] A. Dighe, S. Goswami, and S. Ray, Phys. Rev. D **79**, 076006 (2009).
[49] S. Gupta, S. K. Kang, and C. S. Kim, Nucl. Phys. **B893**, 89 (2015).
[50] J. R. Ellis, A. Hektor, M. Kadastik, K. Kannike, and M. Raidal, Phys. Lett. B **631**, 32 (2005).
[51] J. A. Casas, J. R. Espinosa, A. Ibarra, and I. Navarro, Nucl. Phys. **B569**, 82 (2000).
[52] J. A. Casas, J. R. Espinosa, A. Ibarra, and I. Navarro, Nucl. Phys. **B573**, 652 (2000).
[53] M.-C. Chen and K. T. Mahanthappa, Int. J. Mod. Phys. A **16**, 3923 (2001).
[54] A. S. Joshipura, S. D. Rindani, and N. N. Singh, Nucl. Phys. **B660**, 362 (2003).
[55] R. N. Mohapatra, M. K. Parida, and G. Rajasekaran, Phys. Rev. D **69**, 053007 (2004).
[56] Y. Zhang, X. Zhang, and B.-Q. Ma, Phys. Rev. D **86**, 093019 (2012).
[57] T. Araki, H. Ishida, H. Ishimori, T. Kobayashi, and A. Ogasahara, Phys. Rev. D **88**, 096002 (2013).
[58] W. Wang, Int. J. Mod. Phys. A **29**, 1430040 (2014).
[59] R. L. Arnowitt and P. Nath, Phys. Rev. Lett. **69**, 725 (1992).
[60] Y. Yamada, Z. Phys. C **60**, 83 (1993).
[61] V. D. Barger, M. S. Berger, and P. Ohmann, Phys. Rev. D **47**, 1093 (1993).
[62] N. G. Deshpande and E. Keith, Phys. Rev. D **50**, 3513 (1994).
[63] N. N. Singh and S. B. Singh, Eur. Phys. J. C **5**, 363 (1998).